Peroxiredoxin promotes longevity and H_2O_2-resistance in yeast through redox-modulation of protein kinase A

Friederike Roger[1], Cecilia Picazo[2], Wolfgang Reiter[3], Marouane Libiad[4], Chikako Asami[1], Sarah Hanzén[1], Chunxia Gao[1], Gilles Lagniel[4], Niek Welkenhuysen[5], Jean Labarre[4], Thomas Nyström[6], Morten Grøtli[1], Markus Hartl[3], Michel B. Toledano[4] and Mikael Molin*[1,2]

[1]Department of Chemistry and Molecular Biology, University of Gothenburg, SWEDEN

[2]Department of Biology and Biological Engineering, Chalmers University of Technology, Gothenburg, SWEDEN

[3]Mass Spectrometry Facility, Department of Biochemistry, Max F. Perutz Laboratories, University of Vienna, Vienna BioCenter, Vienna, AUSTRIA

[4]Oxidative Stress and Cancer Laboratory, Integrative Biology and Molecular Genetics Unit (SBIGEM), CEA Saclay, FRANCE

[5]Department of Mathematical Sciences, Chalmers University of Technology and University of Gothenburg, SWEDEN

[6]Department of Microbiology and Immunology, Institute for Biomedicine, Sahlgrenska Academy, University of Gothenburg

*Correspondence: mikael.molin@chalmers.se

Keywords

Aging, peroxiredoxin, H_2O_2 signaling, protein kinase A, glutathionylation, hormesis

Abstract

Peroxiredoxins are H_2O_2 scavenging enzymes that also carry H_2O_2 signaling and chaperone functions. In yeast, the major cytosolic peroxiredoxin, Tsa1 is required for both promoting resistance to H_2O_2 and extending lifespan upon caloric restriction. We show here that Tsa1 effects both these functions not by scavenging H_2O_2, but by repressing the nutrient signaling Ras-cAMP-PKA pathway at the level of the protein kinase A (PKA) enzyme. Tsa1 stimulates sulfenylation of cysteines in the PKA catalytic subunit by H_2O_2 and a significant proportion of the catalytic subunits are glutathionylated on two cysteine residues. Redox modification of the conserved Cys243 inhibits the phosphorylation of a conserved Thr241 in the kinase activation loop and enzyme activity, and preventing Thr241 phosphorylation can overcome the H_2O_2 sensitivity of Tsa1-deficient cells. Results support a model of aging where nutrient signaling pathways constitute hubs integrating information from multiple aging-related conduits, including a peroxiredoxin-dependent response to H_2O_2.

Introduction

Caloric restriction (CR) is an intervention that slows down aging and reduces the incidence of age-related disease from the unicellular baker's yeast (Lin, Defossez, & Guarente, 2000) to rhesus monkeys (Mattison et al., 2017). CR-induced reduced nutrient signaling via insulin/insulin-like growth factor (IGF-1), the target-of-rapamycin and/or protein kinase A pathways is intimately linked to lifespan extension (L. Fontana, Partridge, L., and Longo, V.D., 2010; Kenyon, 2010; Molin & Demir, 2014; Nystrom, Yang, & Molin, 2012). Of other things, reduced nutrient signaling mitigates age-related oxidative damage by increasing oxidative stress resistance in organisms from yeast to humans (Fontan-Lozano, Lopez-Lluch, Delgado-Garcia, Navas, & Carrion, 2008; Heilbronn et al., 2006; Molin et al., 2011; Schulz et al., 2007; Sohal & Forster, 2014). Increased oxidative stress resistance appears as a common denominator of mechanisms by which nutrient signaling pathways dictate the anti-aging effects of CR and its health benefits (Alic & Partridge, 2011; L. Fontana, Partridge, & Longo, 2010; Longo, Shadel, Kaeberlein, & Kennedy, 2012). Still very few specific targets of nutrient signaling that explain the beneficial effects of CR have been identified (L. Fontana et al., 2010).

Peroxiredoxins might constitute one such target, as this major family of peroxide-negating enzymes is required for lifespan promotion by CR and CR-mimetics (De Haes et al., 2014; Molin et al., 2011; Olahova & Veal, 2015). In worms, the CR-mimetic drug metformin extends lifespan in a manner dependent on the activity of Prdx-2 (De Haes et al., 2014), and in flies, neuronal peroxiredoxin overexpression extends lifespan in the absence of caloric restriction (Lee et al., 2009). In addition, CR increases both yeast H_2O_2 tolerance and lifespan by stimulating the activity of the major 2-Cys peroxiredoxin, Tsa1 (Molin et al., 2011), and the mild overexpression of Tsa1 potently extends lifespan [by 40% (Hanzen et al., 2016)]. As peroxiredoxins have been described as major peroxide scavenging enzymes, they may reduce the rate of aging by scavenging H_2O_2, which may also explain their requirement for the maintenance of genome stability (Molin & Demir, 2014; Nystrom et al., 2012) and the premature accumulation of age-related tumors in PrxI-deficient mice (Neumann et al., 2003). However, mild Tsa1 overexpression, although increasing lifespan, did not alter the rate at which mutations accumulate during aging (Hanzen et al., 2016). Furthermore, CR reduced the increased mutation rate in Tsa1-deficient cells by 50% (Hanzen et al., 2016) without extending their life-span (Molin et al., 2011). We instead proposed that Tsa1 counteracts age-related protein damage by guiding Hsp70/104 molecular chaperones to proteins aggregating upon increased age and H_2O_2 (Hanzen et al., 2016).

Prx are obligate dimers carrying two catalytic residues, the peroxidatic Cys (C_P, Cys48 in Tsa1) and the resolving Cys (C_R, Cys171 in Tsa1). C_P reduces H_2O_2 and forms a sulfenic acid (-SOH), which condenses with the C_R of the second Prx molecule into an inter-subunit disulfide, then reduced by thioredoxin. Once formed, the C_P-SOH can also react with another H_2O_2 molecule, which leads to formation of a sulfinic acid ($-SO_2H$), instead of condensing into a disulfide. Sulfinylation inactivates the catalytic cycle, switching the enzyme function into a molecular chaperone by multimerisation (Hanzen et al., 2016; Jang et al., 2004; Noichri et al., 2015). Prxs can also signal H_2O_2 by transfer of the oxidant signal to target proteins (Leichert & Dick, 2015; Stocker, Van Laer, Mijuskovic, & Dick, 2017).

We recently showed that, in response to H_2O_2, Tsa1 and thioredoxin are required for the activation of the transcription factor Msn2, as it inhibits PKA-mediated Msn2 repression (Bodvard et al., 2017). Here we explored whether the modulation of PKA by Tsa1 had any relevance in its role in slowing down aging and in H_2O_2 resistance. We show that both the premature aging and H_2O_2 sensitivity of cells lacking Tsa1 is due to aberrant protein kinase A (PKA) activation, and not to defective H_2O_2 scavenging *per se*. Similarly, a single extra copy of the *TSA1* gene extended life-span by mildly reducing PKA

activity, without affecting H_2O_2 scavenging. Tsa1 interacts with PKA at the level of its catalytic subunits. We identified a conserved Cys residue in the PKA catalytic subunit Tpk1 that is specifically required for Tsa1-mediated H_2O_2 resistance. Tsa1-dependent oxidation of the catalytic subunit reduced enzyme activity and increased H_2O_2 resistance in part through dephosphorylating a conserved threonine (Thr241) in the kinase activation loop. These results indicate that peroxiredoxins slow down the rate of aging through a unique role in kinase signaling, in addition to promote proteostasis. They also suggest a novel mode of regulation of the conserved nutrient-sensing cascade PKA that bypasses conventional signaling via the second messenger cAMP, and impinges on both H_2O_2 resistance and aging.

Results

The effects of Tsa1 on longevity are mediated by the Ras-cAMP-PKA pathway

A single extra-copy of the *TSA1* gene, which encodes the major yeast cytosolic Prx, Tsa1, prolongs lifespan in the absence of caloric restriction (Hanzen et al., 2016). To clarify the mechanism by which Tsa1 promotes this effect, we enquired whether PKA is involved, as this kinase antagonizes both longevity (Lin et al., 2000) and resistance to H_2O_2 (Molin et al., 2011) and Tsa1 is required for decreasing PKA-dependent phosphorylation of the 'general stress' transcription factor Msn2 in response to H_2O_2 (Bodvard et al., 2017). The high affinity cAMP-phosphodiesterase Pde2 degrades cAMP, and deletion of *PDE2* promotes PKA activation by increasing cAMP levels, downstream of Ras2 [Figure 1A, (Broach, 2012; Deprez, Eskes, Wilms, Ludovico, & Winderickx, 2018; Santangelo, 2006)]. Deletion of *PDE2* decreased the lifespan of the wild type strain by 45% (Fig. 1B), as previously shown (Lin et al., 2000), and also prevented the increased lifespan conferred by mild overexpression of *TSA1* (compare *pde2Δ* and *pde2Δ* o/e *TSA1*), which indicates that PKA activity is dominant over Tsa1, and suggests that Tsa1 might slow down aging by decreasing PKA activity. Indeed, mild *TSA1* overexpression increased both the accumulation of the reserve carbohydrate glycogen (Figure 1C), a

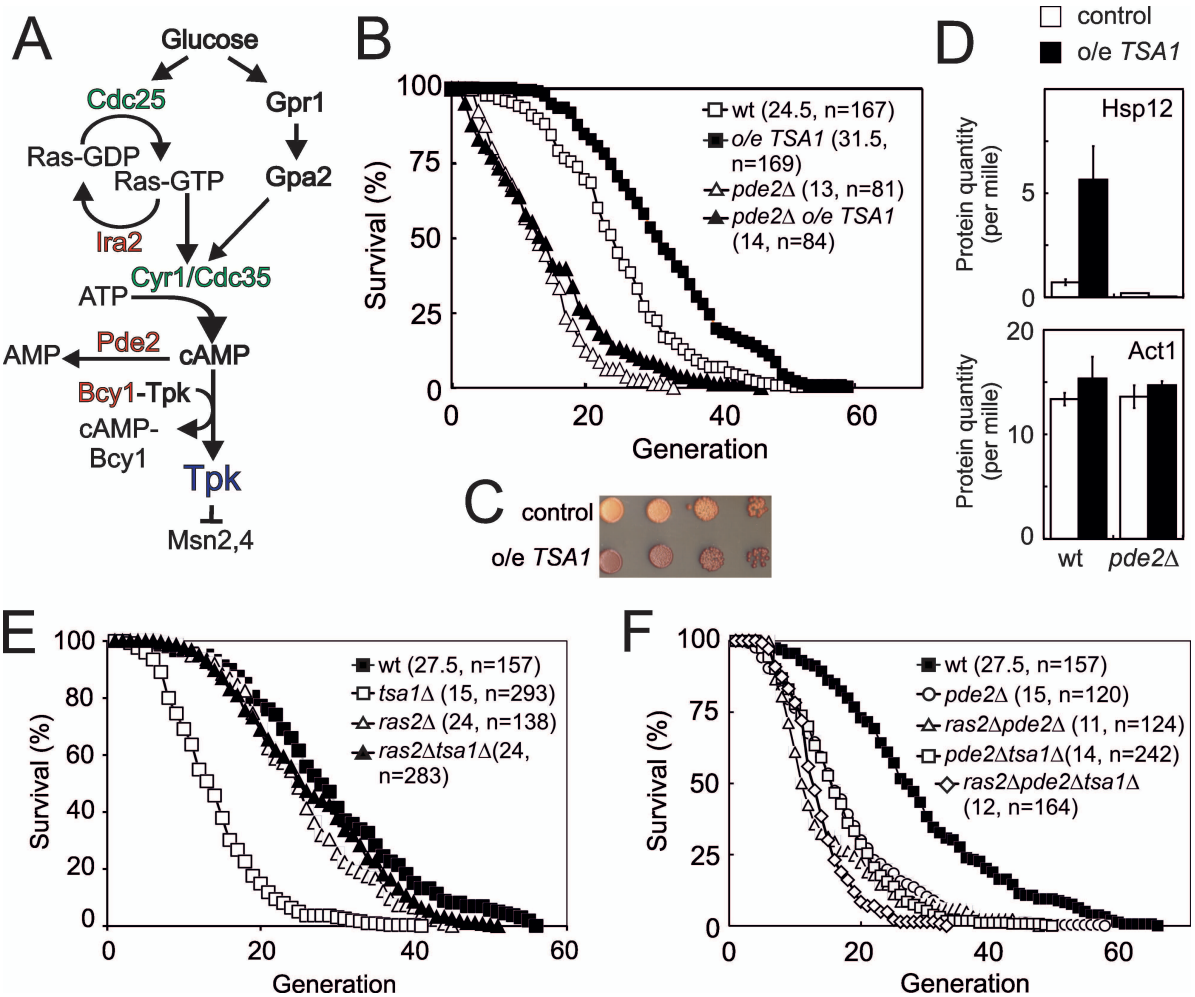

Figure 1. The 2-cys peroxiredoxin Tsa1 slows down aging via inhibiting protein kinase A signaling. **A)** Overview of the Ras-cAMP-PKA signaling pathway. In green stimulatory components and in red inhibitory. **B)** Lifespans of cells expressing an extra copy of the *TSA1* gene or not (vector control) in combination with the deletion of *PDE2* to induce high PKA signaling (*pde2Δ*). **C)** Accumulation of glycogen in vector control cells or cells expressing an extra copy of the *TSA1* gene as assayed by iodine vapor. **D)** Expression of Hsp12 in the indicated mutant strains (n=3). **E-F)** Lifespan of cells lacking Tsa1, Ras2, Pde2 or combinations thereof.

diagnostic feature of low PKA activity, and the expression of the PKA-repressed Msn2/4 target Hsp12 (Figure 1D).

We turned to cells lacking *TSA1*, which suffer a severely shortened lifespan (Molin et al., 2011), asking whether this phenotype is linked to PKA. We combined the deletion of *TSA1* and *RAS2*, the latter largely abrogating the stimulation of PKA by glucose [Figure 1A, (Santangelo, 2006)]. Strikingly, Ras2 deficiency completely rescued the reduced lifespan (Figure 1E) of cells lacking Tsa1, and upon deletion of *PDE2* in these cells (*ras2Δtsa1Δpde2Δ*), this rescue was no longer visible (Figure 1F). These data indicate that the shortened lifespan of *tsa1Δ* is due to aberrant activation of the Ras-PKA pathway, and as a corollary, that Tsa1 might inhibit this pathway. That Tsa1 deletion did not further reduce the lifespan of Pde2-deficient cells (Figure 1F), further support the notion that Tsa1 influences longevity by repressing the Ras-PKA pathway.

Tsa1 represses the Ras-cAMP-PKA pathway at the level of the PKA enzyme

Cells lacking Ras2 grew significantly slower than the wild-type (Figure 2A), consistent with a substantial reduction in PKA activity. However, deleting *TSA1* in these cells (*ras2Δtsa1Δ*) rescued its slow growth to a rate indistinguishable from that of *tsa1Δ* (Figure 2A), again pointing to an antagonistic effect of Tsa1 on the Ras-PKA pathway, also suggesting that Tsa1 affects the pathway downstream of Ras2. Similarly, overexpressing Ira2, a Ras-GTPase activating protein (RasGAP) that decreases PKA activation by switching RAS-GTP to its inactive GDP form, both slowed down growth to approximately half the rate of control cells (Figure 2C) and increased expression of Msn2/4-target genes that are under PKA repression (Figure 2D). Deleting *TSA1* in this strain restored both phenotypes (Figure 2B-D), similar to the effect of Ras-overactivation (*RAS2G19V* allele, Figure 2 – figure supplement 1A-B) or Pde2 deficiency (Figure 2C). Importantly, rescue of the slow growth of Ira2-overproducing cells by Tsa1 deletion was lost when *PDE2* was also overexpressed in these cells, also indicating that the rescue is due to increased PKA activity (Figure 2E).

Strains lacking both *RAS* alleles (*ras1Δras2Δ*) are not viable due to inactivation of PKA. This inability to germinate can be rescued by genetic interventions that restore PKA activity downstream of Ras, i.e. the inactivation of Pde2 or of the PKA negative regulatory subunit Bcy1 (Garrett & Broach, 1989; Toda et al., 1985; Wilson & Tatchell, 1988), or of Yak1, which acts downstream of PKA. Loss of the PKA-repressed 'general stress' transcription factor Msn2 alone or of both Msn2 and its homologue Msn4, can also partially overcome the growth impairment of the partial loss of active Ras (Figure 2C) and the requirement for a PKA catalytic subunit-encoding (*TPK*)-gene for viability (Smith, Ward, & Garrett, 1998). As the above data indicate that Tsa1 represses PKA activity, we tested whether its loss could similarly rescue the inability of *ras1Δras2Δ* to germinate by sporulating heterozygous *ras1Δ/RAS1*, *ras2Δ/RAS2* and *tsa1Δ/TSA1* diploid cells. However, no cells lacking both Ras1 and Ras2 were viable irrespective of the presence or absence of Tsa1 (Figure 2F). Similarly, we did not obtain viable *tsa1Δ tpk1Δ tpk2Δ tpk3Δ* spores in a cross between haploid *tsa1Δ* and *tpk1Δ tpk2Δ tpk3Δ* strains unless a centromeric *TPK1* plasmid was also present (in 6 out of 6 viable spores with the genomic *tsa1Δ tpk1Δ tpk2Δ tpk3Δ* genotype (Figure 2 - figure supplement 1C). These data suggest that the repression exerted by Tsa1 on the Ras-PKA pathway requires the presence of PKA, and thus that the latter may be the target of repression.

To further ascertain at which level Tsa1 interferes with Ras-cAMP-PKA activity, we overproduced the PKA negative regulatory subunit (mc-*BCY1*), which by inactivating PKA releases repression of Msn2, and dramatically increases the latter's response to H_2O_2 (Bodvard et al., 2017) (Figure 2G). However,

mc-*BCY1* had no effect in Tsa1-deficient cells (Figure 2G), suggesting that Tsa1 inhibits the Ras-cAMP-PKA pathway at the level of the PKA enzyme. We also measured the levels of the pathway signaling intermediates, Ras-GTP and cAMP, in cells overproducing Ira2 in the presence and absence of Tsa1. As expected, overexpression of *IRA2* dramatically reduced the levels of active Ras (Ras-GTP) and this reduction was largely maintained in *pde2Δ* cells (Figure 2H), in which PKA signaling is increased downstream of Ras. Similarly, Tsa1-deficient cells overproducing Ira2 exhibited very low Ras-GTP

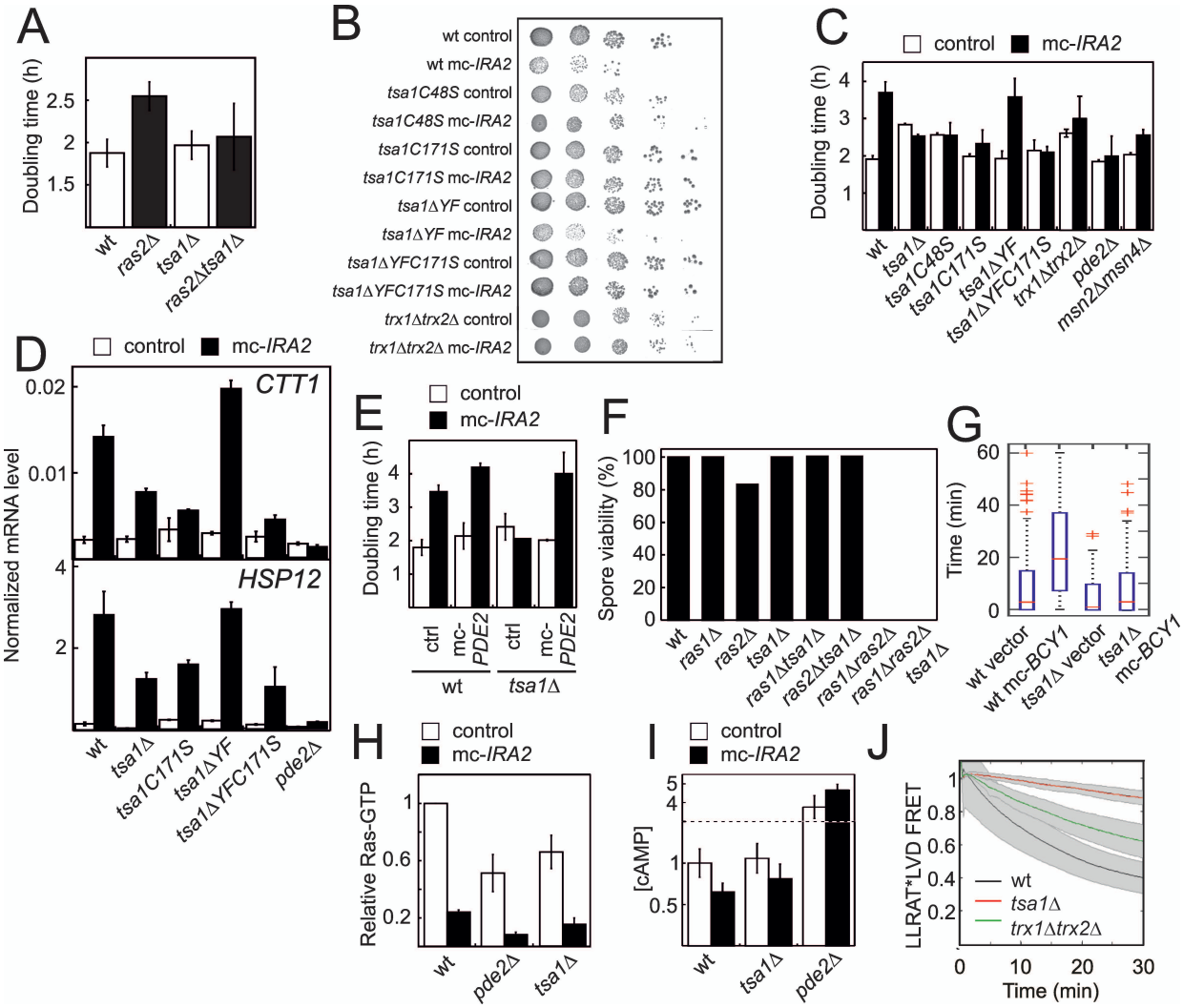

Figure 2. The Tsa1 catalytic cysteines affect protein kinase A dependent proliferation downstream of cAMP but not downstream of the catalytic subunits. **A)** Growth of cells lacking Ras2, Tsa1 or both (n=3, error bars indicate SD). **B-C)** Growth of cells overexpressing *IRA2* in the indicated mutants of the Tsa1 catalytic cycle or the PKA signaling pathway on solid (**B**) or in liquid medium (**C**, n=3-15). **D)** Expression of the PKA repressed *CTT1* or *HSP12* genes in the indicated mutants in the Tsa1 catalytic cycle overexpressing *IRA2* (mc-*IRA2*) or not (instead expressing the vector, control, n=3±SD) sampled during mid-exponential growth. **E)** Growth of Tsa1-proficient or deficient (*tsa1Δ*) cells overexpressing *IRA2* (mc-*IRA2*) or *PDE2* (mc-*PDE2*), both or the corresponding vector control plasmids (control) in liquid medium (n=3±SD). **F)** Spore germination in cells deficient in Ras1, Ras2, Tsa1 or combinations thereof. Spore germination was estimated in 32 tetrads where genotypes could be assigned to all spores (128 in total, 8-23 spores per genotype). **G)** Total time of nuclear Msn2 localization in the indicated mutant strains for 60 min following the addition of 0.3 mM H_2O_2 (n=46-82). **H-I)** Ras-GTP (**H**) or cAMP (**I**) levels in the wild-type or the indicated mutant strains overexpressing *IRA2* (mc-*IRA2*) or not (expressing the vector control, control, n=3). **J**. Phosphorylation of the ectopic AKAR4 PKA site upon H_2O_2 addition (0.4 mM) in wt, *tsa1Δ* and *trx1Δtrx2Δ* cells. (n=85, 71 & 32, respectively). Error bars indicate SD.

levels (Figure 2H). In addition, cAMP levels were not affected in Tsa1-deficient cells (Figure 2I). Altogether, these data indicate that repression of the Ras-cAMP-PKA pathway by Tsa1 is needed both during aging and normal growth, and that this repressive effect is exerted at the level of PKA. Lastly, to directly monitor the impact of Tsa1 on PKA activity, we used a PKA sensor in which the phosphorylation state of the ectopic PKA site LLRAT*-LVD in the mammalian FHA1 phospho-amino acid domain is evaluated via FRET (Molin et al., 2020). PKA repression upon H_2O_2 addition was readily visible in wild-type cells using this sensor, whereas cells lacking Tsa1 hardly repressed PKA at all (Figure 2J).

Altogether, these data indicate that repression of the Ras-cAMP-PKA pathway by Tsa1 is exerted at the level of PKA, and occurs during aging, in the cell response to H_2O_2 and during normal growth.

Tsa1 catalytic cysteines control H_2O_2 resistance by repressing PKA

Prxs can function as H_2O_2 scavengers, as receptors of H_2O_2 signaling relays, or as chaperones. The first two functions require Prx-two catalytic Cys residues C_P and C_R and electrons from thioredoxin, whereas the third one only relies on the sulfinylation of C_P. To sort out which of these three Prx biochemical functions is involved in PKA repression, we examined the effect of mutating C_P and C_R or of preventing enzyme sulfinylation on Tsa1-mediated repression. The lifespans of *tsa1C48S* and *tsa1C171S* mutants suffered a lifespan as short as cells lacking Tsa1 (Figure 3A). Similarly, both the slow growth and the constitutive expression of the PKA-repressed genes *CTT1* and *HSP12* resulting from Ira2 overproduction were lost in the *tsa1C48S* and *tsa1C171S* mutants (Figure 2B-D). In contrast, cells expressing a truncated form of Tsa1 lacking the C-terminal YF motif (*tsa1ΔYF*), an enzyme form almost totally resilient to sulfinylation (Hanzen et al., 2016), were indistinguishable from wild-type with regards to their lifespan (Figure 3A), slow growth and Ira2 overexpression-dependent, constitutive Msn2-target expression (Figure 2B-D), thus excluding an involvement of the Tsa1 chaperone function in PKA repression.

Next, to differentiate between the scavenging and signaling functions of Tsa1, we first probed the H_2O_2 sensitivity phenotype of cells lacking Tsa1. The *tsa1*Δ was sensitive to H_2O_2, as monitored by growth on plates containing H_2O_2, and strikingly, deletion of *RAS2* or the overproduction of Ira2 totally rescued this phenotype (Figure 3B-C). Deletion of *PDE2* in these cells (*ras2Δtsa1Δpde2Δ* or *tsa1Δpde2Δ* mc*–IRA2*) restored the H_2O_2 sensitivity of *tsa1*Δ (Figure 3, figure supplement 1A), further indicating that the *tsa1*Δ H_2O_2 phenotype is linked to overactive PKA, and not to the loss of Tsa1 scavenging function. Similarly, mild overexpression of *TSA1* conferred an increased tolerance to H_2O_2, which was lost upon deletion of *PDE2* (Figure 3D). As another indication of Tsa1 scavenging function dispensability, the decay rate of H_2O_2 in the medium of *tsa1*Δ cells after adding a bolus dose was similar to the rate observed in a wild-type cell suspension (Figure 3F). In addition, H_2O_2 levels measured using the genetically encoded H_2O_2 sensor HyPer3 (Bilan et al., 2013) were modestly, but significantly increased in old wild-type (10-12 generations), relative to young cells (Figure 3G). Tsa1-deficient cells however, exhibited a similar or even lower increase in the H_2O_2 fluorescence ratio with age, relative to wild-type, and in cells expressing an extra copy of the *TSA1* gene, H_2O_2 increased to a similar or even higher levels in aged cells (Figure 3H).

We also examined the role of the thioredoxin pathway in PKA repression, which although required for both Tsa1 signaling and scavenging functions, should be more important for the latter. Deletion of *TRX1* and *TRX2* partly rescued the slow growth of *IRA2*-overexpressing cells (Figure 2B-C), and suppressed the increased constitutive expression of the PKA-repressed Msn2/4 target genes resulting from Ras2 deletion (Figure 2 – figure supplement 1D), the latter even more so than did the deletion of *TSA1*.

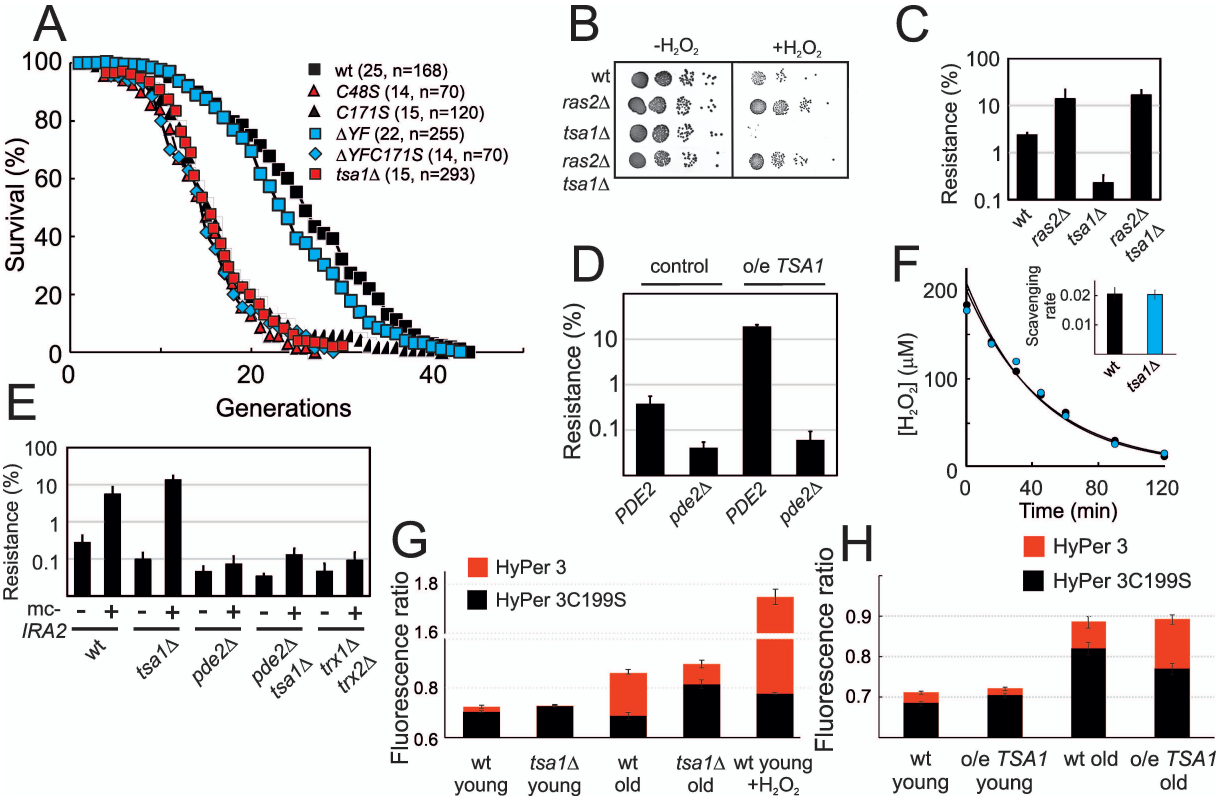

Figure 3. Tsa1 catalytic cysteines slow down aging and increase H_2O_2-resistance via inhibiting protein kinase A. **A.** Life spans of wild-type or the indicated genomic *tsa1* mutant strains. In brackets median life-spans and n. **B.** Spot-test assay of growth in the presence and absence of 1.5 mM H_2O_2 in YPD plates. **C.** Quantification of H_2O_2 resistance in **B** (n=3). **D.** H_2O_2 resistance (1.5 mM H_2O_2, YPD medium) in the indicated mutants (n=3). **E.** H_2O_2 resistance in cells overexpressing *IRA2* (mc-*IRA2* **+**) or vector control (**-**) 0.4 mM H_2O_2, SD medium (n=3). **F.** Culture medium H_2O_2 removal assay of wt (black) and *tsa1Δ* cells (blue) to which 200 μM was added. Inset shows average scavenging rates for cultures upon the addition of 400 μM (n=3). Error bars indicate SD. **G.** Average HyPer3 (red) or HyPer3 C199S (black) fluorescence ratio (500 nm/420 nm) in young or aged wild-type or *tsa1Δ* cells +/- 400 μM H_2O_2 for 10 min. Cells of about 10-12 generations of replicative age (aged) or young control cells (young) were assayed. Error bars indicate SEM (n=231, 170, 319, 236 & 202, respectively). **H.** Average HyPer3 (red) or HyPer3 C199S (black) fluorescence ratio (500 nm/420 nm) in young or aged wild-type (YMM130) and o/e *TSA1* cells as in **G.** Error bars indicate SEM (n=404, 579, 190 & 204, respectively).

However, although H_2O_2 sensitive, this *trx1Δtrx2Δ* strain H_2O_2 phenotype could neither be rescued by deletion of *RAS2* (Figure 3 – figure supplement 1B) nor by the overproduction of Ira2 (Figure 3E). In addition, PKA was still moderately repressed in *trx1Δtrx2Δ* in response to H_2O_2, as measured with the FRET PKA phosphorylation sensor (Figure 2J). Thioredoxins are thus only partially required to repress the phosphorylation of an ectopic PKA target site upon H_2O_2 addition, or may govern signaling through another pathway that synergizes with PKA in some PKA output functions. Nevertheless, that the Tsa1 catalytic Cys residues are critical to restrain PKA activity, but not the thioredoxins further exclude the Tsa1 scavenging function *per se*.

Tpk1 is sulfenylated upon H_2O_2 addition and glutathionylated on the conserved Cys243

If indeed Tsa1 inhibits PKA, we asked by which mechanism this happens. We detected in myc-Tsa1 immunoprecipitates from unstressed cells a weak, but significant amount of Tpk1, the amount of which increased dramatically following H_2O_2 addition (0.4 mM, Figure 4A). Conversely, immunoprecipitating

Tpk1-HB brought down a significant amount of Tsa1 (Figure 4, figure supplement 1A). We next asked whether PKA underwent thiol-redox modifications. Non-reducing electrophoresis did not identify any migration changes compatible with the presence of a disulfide in neither of Tpk1 nor Bcy1 (Figure 4 - figure supplement 1B-C). Similarly, kinetic-based trapping using *tsa1*- and *trx2*-resolving cysteine mutants (*tsa1C171S* and *trx2C34S*) neither altered Bcy1 nor Tpk1 migration (Figure 4 - figure supplement 1B-D). We thus performed a mass spectrometry (MS) analysis using affinity-purified His-biotin-tagged Tpk1 (Tpk1-HB) (Tagwerker et al., 2006) (Supplementary file 2A). We selected a set of peptides covering the most abundant Tpk1 PTMs of its two unique Cys residues, Cys195 and Cys243, and performed a quantitative analysis by label free quantification of MS1 peaks, followed by a targeted MS/MS approach by parallel reaction monitoring (PRM). A significant proportion of Cys195 was present as an adduct with glutathione (GSH) in unstressed cells (Figure 4 – figure supplement 1E, Supplementary file 2B), and levels of all three peptides bearing this modification decreased by 6 and 11-fold upon cell exposure to 0.4 mM and 0.8 mM H_2O_2, respectively (Figure 4 – figure supplement 1F, Supplementary file 2C-2D). A significant fraction of Tpk1 Cys243 was also glutathionylated, even in unstressed cells, and in this peptide, Thr241 was phosphorylated (Figure 4B- C, Figure 4 – figure supplement 1G-H, Supplementary file 2B). We also detected variants of this peptide bearing other cysteine modifications (i.e. methyl thiolation, sulfinylation and unknown modifications, Figure 4 – figure supplement 1G). Importantly, Thr241 phosphorylation decreased upon exposure to H_2O_2 (Figure 4C, Figure 4 – figure supplement 1G), as did Cys243 glutathionylation (2.5-fold), when it occurred on the phosphorylated peptide (Figure 4C). However, the Cys243 glutathionylated Thr241 dephosphorylat-

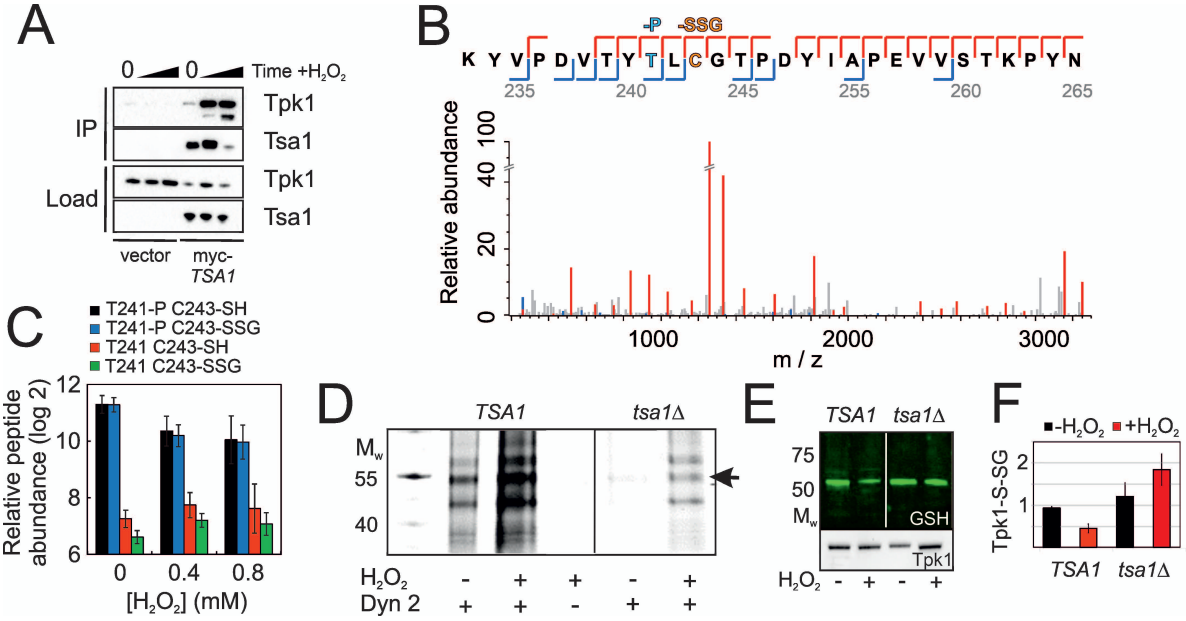

Figure 4. Tsa1 interacts with the PKA catalytic subunit Tpk1 and stimulates Tpk1 cysteine sulfenylation by H_2O_2. Tpk1 is glutathionylated at a conserved cysteine. **A.** Tpk1 interacts with myc-Tsa1 in a coimmunoprecipitation assay and in a manner strongly stimulated by H_2O_2. **B.** MS-MS spectrum showing the matching b-ion (blue) and y-ion (red) series following fragmentation of the Thr241 phosphorylated and C243 glutathionylated peptide encompassing amino acid residues Y239-K261 in Tpk1. T-P = phospho-threonine, C-SSG = glutathionylated cysteine. **C.** PRM-based quantification of the indicated Thr241 and Cys243 containing Y239-K261 peptides in Tpk1, in the absence or presence of the indicated amount of H_2O_2, respectively (n=3). Error bars indicate SD. **D.** DYn-2 assay showing Tpk1 cysteine sulfenylation in the presence and absence of *TSA1* and +/- 0.5 mM H_2O_2 for 5 min. Tpk1-HB was immunoprecipitated from *tpk2Δtpk3Δ (TSA1)* and *tpk2Δtpk3Δtsa1Δ (tsa1Δ)* cells and analyzed in gel for cyanine5 fluorescence. **E-F.** Glutathionylation of Tpk1-HB in strains in **D** as assayed by anti-glutathione immunoblot of immunoprecipitated Tpk1-HB in the absence of or 10 min following the addition of 0.4 mM H_2O_2. Extracts were separated under non-reducing conditions (n=3).

ed peptide increased by 1.4 fold. Confirming MS results, Tpk1 was glutathionylated in unstressed cells, when monitored by anti-glutathione immunoblot of immunoprecipitated Tpk1-HB (Figure 4E-F), and this signal decreased upon exposure to H_2O_2. Further, in *tsa1Δ* cells, the glutathionylation signal was more intense, and did not decrease, but rather increased upon H_2O_2 exposure. We also used DYn-2, a cell-permeable cysteine sulfenic acid (-SOH) probe amenable to click chemistry (Yang et al., 2015) as another approach to probe Tpk1 oxidative modifications. In wild-type unstressed cells, Tpk1 displayed a weak DYn-2 signal, the intensity of which significantly increased upon H_2O_2 addition, whereas in *tsa1Δ* cells this signal was much less intense, both prior to and after exposure to H_2O_2 (0.4 mM, Figure 4D, Figure 4 – figure supplement 1I).

The two Tpk1 Cys residues thus undergo complex redox changes comprising glutathionylation and sulfenylation as dominant and biologically relevant modifications. These changes occur independently, the former present in unstressed cells, decreasing upon H_2O_2 exposure, and the latter strongly induced by H_2O_2, both dependent upon Tsa1. The fact that the increased sulfenylation of Tpk1 upon H_2O_2 addition correlates with Thr241 dephosphorylation led us to probe the importance of all three residues in Tpk1 function by Ala substitution. These substitutions altered neither protein levels not the cell ability to grow (Figure 5 – figure supplement 1A-D). Interestingly, *tpk1C243A*, but not *tpk1C195A* rendered cells hyper-sensitive to H_2O_2 (Figure 5A, Figure 5 – figure supplement 1E), which was not improved by mild overexpression of *TSA1* (Figure 5B). In contrast, the *tpk1T241A* mutant significantly increased H_2O_2 resistance both in wild-type (Figure 5A) and in *tsa1*Δ cells (Figure 5C). A docking experiment performed on a Tpk1 3D structural homology model based on the mouse enzyme structure (Figure 5D-E), showed that introducing a glutathione moiety at Cys243 stabilized Thr241 in the dephosphorylated state by direct hydrogen bonding (Figure 5F-H). When Thr241 was phosphorylated, the kinase activation loop was now stabilized through hydrogen bonds to Arg209 and Lys233 (Figure 5F-G), and in this setting, glutathione at Cys243 adopted a different position, now extending towards the ATP-binding pocket (Figure 5I). Subsitution of Cys243 to the less bulky cysteine sulfenic/sulfinic acid mimetic aspartate (*tpk1C243D*), or modification by methylthiolation (S-CH_3, Figure 4 – figure supplement 1E) had, however, little effect on the molecular dynamics of Tpk1 (Figure 5 – figure supplement 1F-G). In summary, Cys243 glutathionylation might inhibit PKA by interfering both with Thr241 phosphorylation and with the ATP-binding pocket dynamics, when occurring together with phosphorylated Thr241, which would not fit the observed decreased glutathionylation of Tpk1 seen upon H_2O_2 addition. Alternatively, the Cys243 sulfenic acid may react further as previously speculated for the redox modulation of the ER kinase IRE-1 (Hourihan, Moronetti Mazzeo, Fernandez-Cardenas, & Blackwell, 2016) and our 3D data suggest that a more bulky modification may be the driving event in PKA repression. Taken together, these data support the presence of a Tsa1 thiol-based redox mechanism in PKA repression.

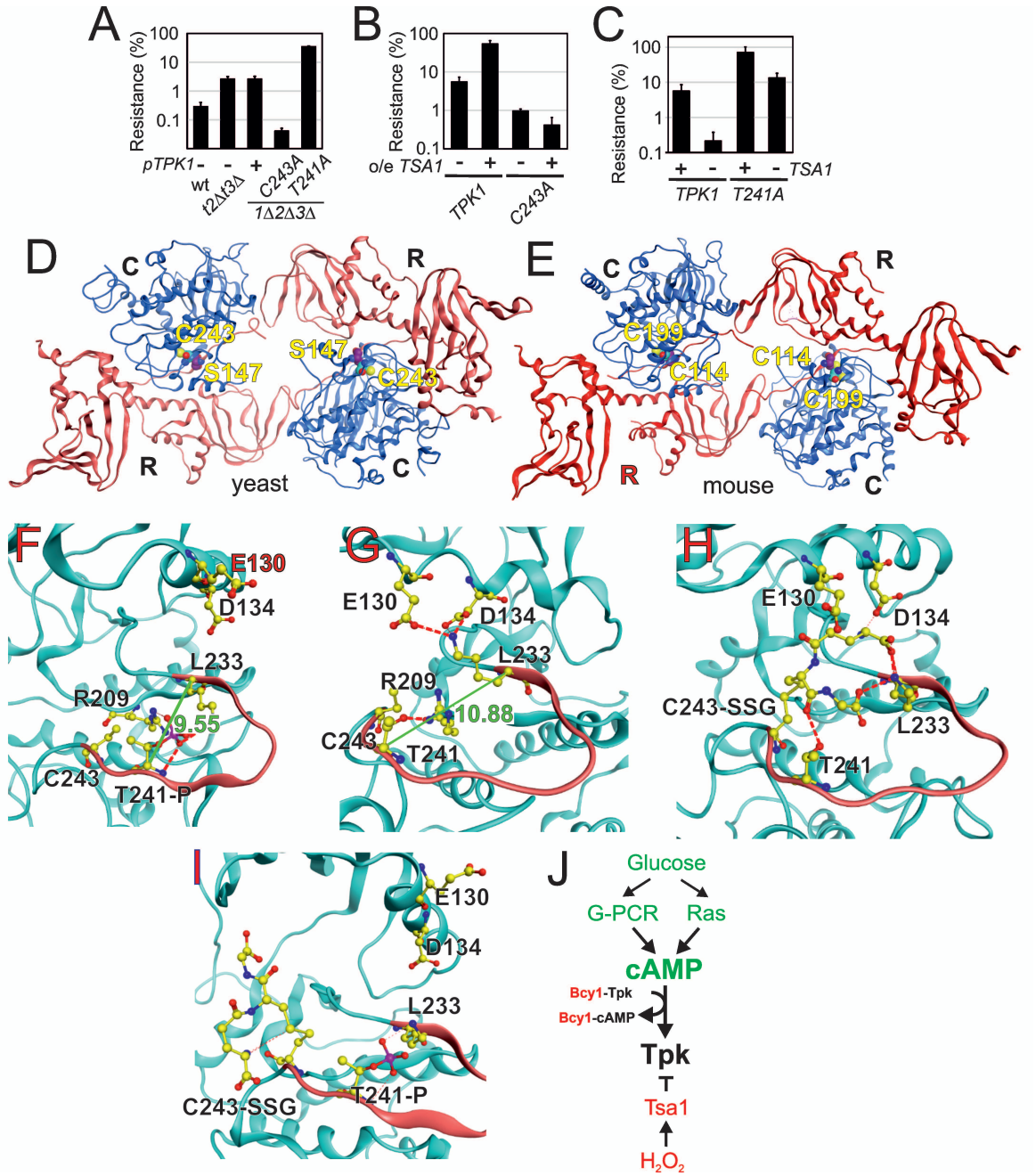

Figure 5. Tpk1 Cys243 redox-modification and Tsa1 inhibits PKA activity by dephosphorylating and destabilizing the activation loop. **A-B.** H_2O_2 resistance of the wild-type vector control (**A**, pRS313 or **B**, pRS403) or the indicated *tsa1*- or *tpk*-mutant strains in SD medium, 0.6 mM H_2O_2. Strains in **B.** carry pRS316-*TPK1* or pRS316-*tpk1C243A* as the only PKA catalytic subunit (genomic *tpk1Δtpk2Δtpk3Δ* deletions, n=3). **C.** H_2O_2 resistance of *tpk1Δtpk2Δtpk3Δ* and *tpk1Δtpk2Δtpk3Δtsa1Δ* cells transformed with pRS313-*TPK1* or pRS313-*tpk1T241A* as indicated in SD medium 0.6 mM H_2O_2 (n=3). **D-E.** Structural homology model of yeast Tpk1 (**D**) based on the structure of mouse type II PKA holoenzyme (**E**) [PDB ID 3TNP, (P. Zhang et al., 2012)]. **F-I.** Amino acids in the activation loop (in red) of Tpk1 in the Thr241 phosphorylated Cys243 non-modified (**F**), Thr241 non-phosphorylated Cys243 non-modified (**G**), Thr241 non-modified Cys243 glutathionylated (**H**) and Thr241 phosphorylated Cys243 glutathionylated (**I**) states in the Tpk1 structural homology model. The backbones are colored in light blue, carbon atoms in yellow, nitrogen atoms in blue, oxygen atoms in red and phosphor atoms in scarlet. The distance between Lys233 and phosphorylated Thr241 is 9.55 Å (**F**) whereas Lys233 and non-phosphorylated Thr241 reside 10.88 Å apart (**G**). *tpk2Δtpk3Δtsa1Δ (tsa1Δ)* as assayed by anti-glutathione immunoblot of immunoprecipitated Tpk1-HB in the absence of or 10 min following the addition of 0.4 mM H_2O_2. Extracts were separated under non-reducing (NR) or reducing (R) conditions. **J.** Overview of mechanisms by which glucose and H_2O_2 control PKA activity. In green activators and in red inhibitors. See also **Figure 5 – figure supplement 1**.

Discussion

Caloric restriction is established as a measure that extends the lifespan of organisms from yeast to primates and this effect occurs by reduced nutrient and/or growth signaling through the insulin/IGF-1, TOR and protein kinase A pathways. However, which effectors/processes downstream of these pathways are regulating the rate of aging is still a matter of controversy. As nutrient signaling coordinates many different cellular processes, the exact identity of the accountable process may differ between organisms and/or CR protocols (Lamming & Anderson, 2014). The fact that several of the target processes proposed, as for instance vacuolar pH control and protein homeostasis, reciprocally feed-back control nutrient signaling (Molin & Demir, 2014; Yao et al., 2015; N. Zhang, Quan, Rash, & Oliver, 2013) has caused further obscured the designation of mechanisms important in slowing down aging. A novel integrative model of aging, however, posits that different pathways and/or organelles are intricately interconnected into so called integrons (Dillin, Gottschling, & Nystrom, 2014), the interconnectivity of which eventually causes a progressive decline of all systems through sequential collapse of homeostasis, when individual subsystems fail.

Peroxiredoxins have emerged as regulators of aging stimulating longevity in organisms from yeast to worms, flies and mice (De Haes et al., 2014; Hanzen et al., 2016; Lee et al., 2009; Molin et al., 2011; Olahova & Veal, 2015). We previously showed that the yeast peroxiredoxin Tsa1 is crucial for molecular chaperones to bind to aggregates forming in aged yeast cells (Hanzen et al., 2016), thus connecting peroxiredoxins to an aging factor conserved in many organisms. We linked this role to the sulfinylation of the enzyme primary catalytic cysteine and protein decamerization, thus providing a demonstration of the *in vivo* occurrence of this *in vitro*-described peroxiredoxin chaperone function (Jang et al., 2004; Noichri et al., 2015). We also previously observed that H_2O_2 resistance in CR cells requires both catalytic cysteines (Molin et al., 2011), and metformin, which extends lifespan in worms, causes the accumulation of disulfide-linked Prdx-2 in worms. These data indicated that handling protein aggregates might not be the only means by which peroxiredoxins regulate aging. Data reported in this study now demonstrate a key role of both cysteines of Tsa1 in slowing down aging, also correlating peroxiredoxin-stimulated longevity and hydrogen peroxide resistance. Surprisingly, the requirement for peroxiredoxin-catalytic cysteines in both aging and H_2O_2 resistance is not linked to H_2O_2 scavenging, but to the modulation of PKA. Taken together with the Tsa1-dependent increased lifespan in cells grown in the continuous presence of low levels of H_2O_2 (Goulev et al., 2017), these data demonstrate that one of the anti-aging effects of peroxiredoxins originates in H_2O_2 signaling. Accordingly, what are the phenotypes dependent on the scavenging function of Tsa1, and of peroxiredoxins in general? Compelling arguments for local scavenging by mouse PrdxI that modulate growth factor signaling have been made (Woo et al., 2010), but literature too often equate a requirement of peroxiredoxin catalytic cysteines with a role of the enzyme in scavenging. Our data now indicate that peroxiredoxins, when bearing its two catalytic residue, can override conventional second-messenger controlled signaling mechanisms to directly modulate protein kinase A signaling as a function of the level of H_2O_2 (Figure 5J).

How is this modulation of PKA by Tsa1 occuring? Our data provide evidence for a direct Tsa1-Tpk1 physical interaction, Tsa1-dependent Tpk1 cysteine sulfenylation and deglutathionylation, and a requirement of Cys243 in H_2O_2 resistance mediated by mild Tsa1 overexpression. Murine type II PKA is inactivated upon *in vitro* glutathionylation of the homologous Cys residue (C199) (Humphries, Deal, & Taylor, 2005; Humphries, Juliano, & Taylor, 2002). In type II rat PKA, the same Cys residue forms a disulfide bond with the regulatory subunit at very low levels of H_2O_2 *in vitro* (1 µM), which decreases PKA activity (de Pina et al., 2008), again highlighting the importance of this residue in PKA redox regulation. The PKA regulatory subunit cysteine is however, only conserved in vertebrates, in contrast

to the catalytic subunit cysteine, which is conserved in PKA across eukaryotes (de Pina et al., 2008). How does PKA then become redox modified? Are glutathionylation and sulfenylation of the PKA catalytic Cys residues, mechanistically linked, and if so which of them occurs first? Peroxiredoxins can oxidize other proteins by virtue of promiscuity, but disulfide bond formation and not sulfenylation is expected to occur in this case (Stocker, Maurer, Ruppert, & Dick, 2018). Furthermore, we could not identify a Tpk1-Tsa1 mixed disulfide by kinetic trapping using a Tsa1 mutant lacking its resolving cysteine (Figure 4 -figure supplement 1A-C). Protein glutathionylation can occur non-enzymatically by condensation with a preformed sulfenate, a mechanism that may explain Tpk1 glutathionylation, but can also be catalyzed by a glutathione-S-transferase (J. Zhang, Ye, Singh, Townsend, & Tew, 2018). A pressing issue for the future will thus be to identify the mechanism by which Tpk1 becomes sulfenylated and glutathionylated and how peroxiredoxins, or possibly other redox enzymes assist these modifications.

The activities of both protein kinase G and A (PKARIα) are also stimulated by H_2O_2 (Burgoyne et al., 2007; Burgoyne et al., 2015). In the protein kinase G Iα isoform, a disulfide linking its two subunits forms in rat cells exposed to H_2O_2 (Burgoyne et al., 2007). Thus this regulation of PKA/PKG by H_2O_2 involves the same Cys195 conserved cysteine in the catalytic subunit but leads to opposite effects. Similarly, *in vitro* studies suggest that the energy-sensing kinase AMPK is activated upon glutathionylation (Klaus et al., 2013). In worms and mammals, the endoplasmic reticulum (ER) transmembrane kinase Ire-1 is regulated by oxidation of another conserved Cys residue in the activation loop, situated 11 residues upstream of the here described PKA cysteine, at position +2 relative to the Mg^{2+}-coordinating DFG motif (Hourihan et al., 2016). Furthermore, we recently found that another activation loop cysteine, positioned at DFG -1, in the fission yeast MAPKK, Wis1, restrains Wis1 activation by low levels, but not high, levels of H_2O_2 (Sjölander et al., 2020). These studies, together with the one presented here, pinpoint oxidation of cysteines in kinase activation loops as prevalent means of fine-tuning protein kinase function in response to H_2O_2.

In summary data presented here and in a previous study (Hanzen et al., 2016) point to two different independent mechanisms by which peroxiredoxins counteract aging and age-related disease (Figure 6). The first one, described here, involves catalytic cycling and inhibition of nutrient-related kinase signaling (Figure 6A-B). This mechanism appears critical for yeast to sustain normal longevity and is probably involved also in the ability of CR to slow down aging, since CR stimulates H_2O_2 resistance in a manner dependent on Tsa1 catalytic cysteines (Molin et al., 2011). Along the same lines, metformin-stimulated longevity in worms also seems to involve increased Prdx-2 disulfide bond formation (De Haes et al., 2014). The second mechanism is the stimulation of chaperone-dependent protein quality control that counteract protein aggregation [Figure 6C, (Hanzen et al., 2016)]. Tsa1 sulfinylation is necessary to guide the molecular chaperones Hsp70 and Hsp104 to aggregates forming in aged and H_2O_2-treated cells. The requirement of both reduced PKA nutrient signaling and normal protein quality control (Hanzen et al., 2016) for mild Tsa1 overproduction to extend lifespan support a requirement of both these mechanisms for enhanced peroxiredoxin levels to extend lifespan (Figure 6C).

Cellular components and/or pathways that assimilate information from different subsystems, such as the above described nutrient signaling pathways, would thus be expected to have a key role as integrating hubs in the aging process. A role of PKA in integrating yeast homeostatic processes is also suggested by a genome-wide identification of genes controlling PKA regulatory-catalytic subunit interaction, and hence PKA activity, which found a striking number of known PKA targets, involved in glycogen accumulation, filamentous growth and amino-acid biosynthesis (Filteau et al., 2015). The role of peroxiredoxins of slowing down aging by modulating central nutrient signaling pathways agrees with

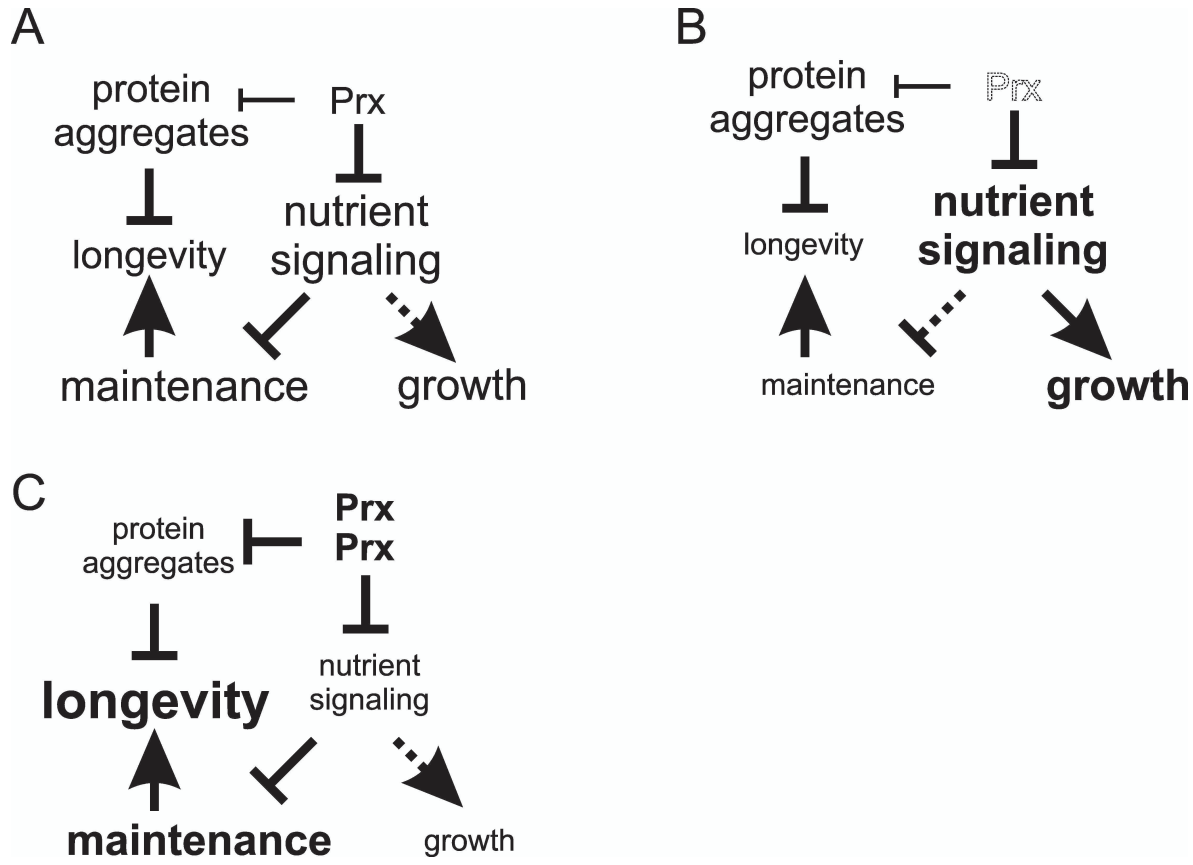

Figure 6. Model of the mechanisms by which altered peroxiredoxin levels impacts on aging. In the first mechanism peroxiredoxin-dependent redox-signaling impacts in an unconventional manner on the PKA nutrient signaling kinase (this study) and in the other on proteostasis (Hanzen et al., 2016). **A)** In wild-type cells Tsa1 catalytic cycling maintains longevity by decreasing PKA-dependent nutrient signaling leading to the stimulation of maintenance but at the expense of growth. **B)** In cells lacking Tsa1, nutrient signaling is aberrantly increased leading to reduced maintenance and increased growth. **C)** Enforced expression of the peroxiredoxin Tsa1 slows down aging both by repressing nutrient signaling (this study) and by stimulating protein quality control mechanisms to reduce the levels of damaged and aggregated protein (Hanzen et al., 2016).

the integrative model of aging and suggest that also other anti-aging regimens might impact nutrient signaling.

The incidence of many major age-related diseases, such as cancer, diabetes and neurodegeneration, can be reduced by caloric restriction (Mattison et al., 2017), and there is hope that reducing caloric intake or pharmaceutically targeting key molecular mechanisms underlying its beneficial health effects, such as peroxiredoxins, will fuel healthy, disease-free ageing. As peroxiredoxins are conserved in organisms from bacteria to humans and can be targeted pharmaceutically, they constitute promising targets for the development of drugs against age-related disease.

Acknowledgements

We are grateful to Karin Voordeckers, Joseph Heitman and Robert J Deschenes for reagents and Mattias Johansson and Lainy Ramirez for technical assistance.

Funding

This work was supported by grants from the Swedish research Council VR, Cancerfonden, the Foundation Olle Engkvist byggmästare and Carl Tryggers stiftelse to MM, and ANR PrxAge and

ERRed2 to MBT. The funding sources had no role in study design, data collection and interpretation or the decision to submit for publication.

Competing interests

The authors declare that they have no conflict of interest.

Author contributions

Conceptualization M.M.; Methodology M.M., W.R., M.H., C.G., N.W., J.L.; Investigation F.R., C.P., M.M., C.A., S.H., G.L., M.L.; Writing – original draft preparation M.M., F.R.; Writing – review and editing, M.B.T, M.M., F.R., T.N., W.R., M.G.; Project administration M.M., Supervision, M.M., M.G.

References

Abraham, M. J., Murtola, T., Schultz, R., Pall, S., Smith, J. C., Hess, B., & Lindahl, E. (2015). GROMACS: High performance molecular simulations through multi-level parallelism from laptops to supercomputers. *SoftwareX, 54*(7), 1932-1940.

Alic, N., & Partridge, L. (2011). Death and dessert: nutrient signalling pathways and ageing. *Curr Opin Cell Biol, 23*(6), 738-743. doi:10.1016/j.ceb.2011.07.006

Berendsen, H. J. C., Postma, J. P. M., Vangunsteren, W. F., Dinola, A., & Haak, J. R. (1984). Molecular-Dynamics with Coupling to an External Bath. *Journal of Chemical Physics, 81*(8), 3684-3690. doi:Doi 10.1063/1.448118

Bilan, D. S., Pase, L., Joosen, L., Gorokhovatsky, A. Y., Ermakova, Y. G., Gadella, T. W. J., . . . Belousov, V. V. (2013). HyPer-3: A Genetically Encoded H2O2 Probe with Improved Performance for Ratiometric and Fluorescence Lifetime Imaging. *ACS chemical biology, 8*(3), 535-542. doi:10.1021/cb300625g

Biteau, B., Labarre, J., & Toledano, M. B. (2003). ATP-dependent reduction of cysteine-sulphinic acid by *S. cerevisiae* sulphiredoxin. *Nature, 425*(6961), 980-984.

Bodvard, K., Peeters, K., Roger, F., Romanov, N., Igbaria, A., Toledano, M. B., . . . Molin, M. (2017). Light-sensing via hydrogen peroxide and a peroxiredoxin. *Nat Commun, 8*, 14791. doi:10.1038/ncomms14791

Broach, J. R. (2012). Nutritional control of growth and development in yeast. *Genetics, 192*(1), 73-105. doi:10.1534/genetics.111.135731

Burgoyne, J. R., Madhani, M., Cuello, F., Charles, R. L., Brennan, J. P., Schroder, E., . . . Eaton, P. (2007). Cysteine redox sensor in PKGIa enables oxidant-induced activation. *Science, 317*(5843), 1393-1397. doi:10.1126/science.1144318

Burgoyne, J. R., Rudyk, O., Cho, H. J., Prysyazhna, O., Hathaway, N., Weeks, A., . . . Eaton, P. (2015). Deficient angiogenesis in redox-dead Cys17Ser PKARIalpha knock-in mice. *Nat Commun, 6*, 7920. doi:10.1038/ncomms8920

Caballero, A., Ugidos, A., Liu, B., Oling, D., Kvint, K., Hao, X., . . . Nystrom, T. (2011). Absence of mitochondrial translation control proteins extends life span by activating sirtuin-dependent silencing. *Molecular cell, 42*(3), 390-400. doi:10.1016/j.molcel.2011.03.021

Colombo, S., & Martegani, E. (2014). Methods to study the Ras2 protein activation state and the subcellular localization of Ras-GTP in Saccharomyces cerevisiae. *Methods Mol Biol, 1120*, 391-405. doi:10.1007/978-1-62703-791-4_24

Costanzo, M., Baryshnikova, A., Bellay, J., Kim, Y., Spear, E. D., Sevier, C. S., . . . Boone, C. (2010). The genetic landscape of a cell. *Science, 327*(5964), 425-431. doi:10.1126/science.1180823

Darden, T., York, D., & Pedersen, L. (1993). Particle Mesh Ewald - an N.Log(N) Method for Ewald Sums in Large Systems. *Journal of Chemical Physics, 98*(12), 10089-10092. doi:Doi 10.1063/1.464397

De Haes, W., Frooninckx, L., Van Assche, R., Smolders, A., Depuydt, G., Billen, J., . . . Temmerman, L. (2014). Metformin promotes lifespan through mitohormesis via the peroxiredoxin PRDX-2. *Proc Natl Acad Sci U S A, 111*(24), E2501-2509. doi:10.1073/pnas.1321776111

de Pina, M. Z., Vazquez-Meza, H., Pardo, J. P., Rendon, J. L., Villalobos-Molina, R., Riveros-Rosas, H., & Pina, E. (2008). Signaling the signal, cyclic AMP-dependent protein kinase inhibition by insulin-formed H2O2 and reactivation by thioredoxin. *J Biol Chem, 283*(18), 12373-12386. doi:10.1074/jbc.M706832200

Deprez, M. A., Eskes, E., Wilms, T., Ludovico, P., & Winderickx, J. (2018). pH homeostasis links the nutrient sensing PKA/TORC1/Sch9 menage-a-trois to stress tolerance and longevity. *Microb Cell, 5*(3), 119-136. doi:10.15698/mic2018.03.618

Depry, C., & Zhang, J. (2011). Using FRET-based reporters to visualize subcellular dynamics of protein kinase A activity. *Methods Mol Biol, 756*, 285-294. doi:10.1007/978-1-61779-160-4_16

Dillin, A., Gottschling, D. E., & Nystrom, T. (2014). The good and the bad of being connected: the integrons of aging. *Curr Opin Cell Biol, 26*, 107-112. doi:10.1016/j.ceb.2013.12.003

Essmann, U., Perera, L., Berkowitz, M. L., Darden, T., Lee, H., & Pedersen, L. G. (1995). A Smooth Particle Mesh Ewald Method. *Journal of Chemical Physics, 103*(19), 8577-8593. doi:Doi 10.1063/1.470117

Filteau, M., Diss, G., Torres-Quiroz, F., Dube, A. K., Schraffl, A., Bachmann, V. A., . . . Landry, C. R. (2015). Systematic identification of signal integration by protein kinase A. *Proc Natl Acad Sci U S A, 112*(14), 4501-4506. doi:10.1073/pnas.1409938112

Fontan-Lozano, A., Lopez-Lluch, G., Delgado-Garcia, J. M., Navas, P., & Carrion, A. M. (2008). Molecular bases of caloric restriction regulation of neuronal synaptic plasticity. *Mol Neurobiol, 38*(2), 167-177.

Fontana, L., Partridge, L., & Longo, V. D. (2010). Extending healthy life span--from yeast to humans. *Science, 328*(5976), 321-326. doi:10.1126/science.1172539

Fontana, L., Partridge, L., and Longo, V.D. (2010). Dietary Restriction, Growth Factors and Aging: from yeast to humans. *Science, 328*(5679), 321-326.

Garrett, S., & Broach, J. (1989). Loss of Ras activity in Saccharomyces cerevisiae is suppressed by disruptions of a new kinase gene, YAKI, whose product may act downstream of the cAMP-dependent protein kinase. *Genes Dev, 3*(9), 1336-1348.

Giaever, G., Chu, A. M., Ni, L., Connelly, C., Riles, L., Veronneau, S., . . . Johnston, M. (2002). Functional profiling of the *Saccharomyces cerevisiae* genome. *Nature, 418*(6896), 387-391.

Goldstein, A. L., & McCusker, J. H. (1999). Three new dominant drug resistance cassettes for gene disruption in *Saccharomyces cerevisiae*. *Yeast, 15*(14), 1541-1553.

Goulev, Y., Morlot, S., Matifas, A., Huang, B., Molin, M., Toledano, M., & Charvin, G. (2017). Nonlinear feedback drives homeostatic plasticity in H2O2 stress response. *Elife, 6*, 23791. doi:http://dx.doi.org/10.7554/eLife.23971

Gueldener, U., Heinisch, J., Koehler, G. J., Voss, D., & Hegemann, J. H. (2002). A second set of loxP marker cassettes for Cre-mediated multiple gene knockouts in budding yeast. *Nucleic Acids Res, 30*(6), e23.

Hanzen, S., Vielfort, K., Yang, J., Roger, F., Andersson, V., Zamarbide-Fores, S., . . . Nystrom, T. (2016). Lifespan Control by Redox-Dependent Recruitment of Chaperones to Misfolded Proteins. *Cell, 166*(1), 140-151. doi:10.1016/j.cell.2016.05.006

Heilbronn, L. K., de Jonge, L., Frisard, M. I., DeLany, J. P., Larson-Meyer, D. E., Rood, J., . . . Pennington, C. T. (2006). Effect of 6-month calorie restriction on biomarkers of longevity, metabolic adaptation, and oxidative stress in overweight individuals: a randomized controlled trial. *JAMA, 295*(13), 1539-1548. doi:10.1001/jama.295.13.1539

Hess, B., Bekker, H., Berendsen, H. J. C., & Fraaije, J. G. E. M. (1997). LINCS: A linear constraint solver for molecular simulations. *Journal of Computational Chemistry, 18*(12), 1463-1472. doi:Doi 10.1002/(Sici)1096-987x(199709)18:12<1463::Aid-Jcc4>3.0.Co;2-H

Hoover, W. G. (1985). Canonical Dynamics - Equilibrium Phase-Space Distributions. *Physical Review A, 31*(3), 1695-1697. doi:DOI 10.1103/PhysRevA.31.1695

Hourihan, J. M., Moronetti Mazzeo, L. E., Fernandez-Cardenas, L. P., & Blackwell, T. K. (2016). Cysteine Sulfenylation Directs IRE-1 to Activate the SKN-1/Nrf2 Antioxidant Response. *Mol Cell, 63*(4), 553-566. doi:10.1016/j.molcel.2016.07.019

Humphries, K. M., Deal, M. S., & Taylor, S. S. (2005). Enhanced dephosphorylation of cAMP-dependent protein kinase by oxidation and thiol modification. *J Biol Chem, 280*(4), 2750-2758. doi:10.1074/jbc.M410242200

Humphries, K. M., Juliano, C., & Taylor, S. S. (2002). Regulation of cAMP-dependent protein kinase activity by glutathionylation. *J Biol Chem, 277*(45), 43505-43511. doi:10.1074/jbc.M207088200

Jacobson, M. P., Friesner, R. A., Xiang, Z., & Honig, B. (2002). On the role of the crystal environment in determining protein side-chain conformations. *J Mol Biol, 320*(3), 597-608.

Jang, H. H., Lee, K. O., Chi, Y. H., Jung, B. G., Park, S. K., Park, J. H., . . . Lee, S. Y. (2004). Two enzymes in one; two yeast peroxiredoxins display oxidative stress-dependent switching from a peroxidase to a molecular chaperone function. *Cell, 117*(5), 625-635.

Kenyon, C. J. (2010). The genetics of ageing. *Nature, 464*(7288), 504-512. doi:nature08980 [pii] 10.1038/nature08980

Klaus, A., Zorman, S., Berthier, A., Polge, C., Ramirez, S., Michelland, S., . . . Schlattner, U. (2013). Glutathione S-transferases interact with AMP-activated protein kinase: evidence for S-glutathionylation and activation in vitro. *PLoS One, 8*(5), e62497. doi:10.1371/journal.pone.0062497

Kong, A. T., Leprevost, F. V., Avtonomov, D. M., Mellacheruvu, D., & Nesvizhskii, A. I. (2017). MSFragger: ultrafast and comprehensive peptide identification in mass spectrometry-based proteomics. *Nat Methods, 14*(5), 513-520. doi:10.1038/nmeth.4256

Lamming, D. W., & Anderson, R. M. (2014). Metabolic Effects of Caloric Restriction. In *eLS*: John Wiley & Sons, Ltd.

Lee, K. S., Iijima-Ando, K., Iijima, K., Lee, W. J., Lee, J. H., Yu, K., & Lee, D. S. (2009). JNK/FOXO-mediated neuronal expression of fly homologue of peroxiredoxin II reduces oxidative stress and extends life span. *J Biol Chem, 284*(43), 29454-29461. doi:M109.028027 [pii] 10.1074/jbc.M109.028027

Leichert, L. I., & Dick, T. P. (2015). Incidence and physiological relevance of protein thiol switches. *Biol Chem, 396*(5), 389-399. doi:10.1515/hsz-2014-0314

Lin, S. J., Defossez, P. A., & Guarente, L. (2000). Requirement of NAD and SIR2 for life-span extension by calorie restriction in Saccharomyces cerevisiae. *Science, 289*(5487), 2126-2128.

Longo, V. D., Shadel, G. S., Kaeberlein, M., & Kennedy, B. (2012). Replicative and chronological aging in Saccharomyces cerevisiae. *Cell metabolism, 16*(1), 18-31. doi:10.1016/j.cmet.2012.06.002

Longtine, M. S., McKenzie, A., 3rd, Demarini, D. J., Shah, N. G., Wach, A., Brachat, A., . . . Pringle, J. R. (1998). Additional modules for versatile and economical PCR-based gene deletion and modification in Saccharomyces cerevisiae. *Yeast, 14*(10), 953-961. doi:10.1002/(SICI)1097-0061(199807)14:10<953::AID-YEA293>3.0.CO;2-U

Mashhoon, N., Carmel, G., Pflugrath, J. W., & Kuret, J. (2001). Structure of the unliganded cAMP-dependent protein kinase catalytic subunit from Saccharomyces cerevisiae. *Arch Biochem Biophys, 387*(1), 11-19. doi:10.1006/abbi.2000.2241

Mattison, J. A., Colman, R. J., Beasley, T. M., Allison, D. B., Kemnitz, J. W., Roth, G. S., . . . Anderson, R. M. (2017). Caloric restriction improves health and survival of rhesus monkeys. *Nat Commun, 8*, 14063. doi:10.1038/ncomms14063

Molin, M., & Demir, A. B. (2014). Linking Peroxiredoxin and Vacuolar-ATPase Functions in Calorie Restriction-Mediated Life Span Extension. *Int J Cell Biol, 2014*, 12. doi:10.1155/2014/913071

Molin, M., Logg, K., Bodvard, K., Peeters, K., Forsmark, A., Roger, F., . . . Blomberg, A. (2020). cAMP-dependent protein kinase controls the multifacteted biology of visible light. *BMC Biology, under review*.

Molin, M., Yang, J., Hanzen, S., Toledano, M. B., Labarre, J., & Nystrom, T. (2011). Life span extension and H_2O_2-resistance elicited by caloric restriction require the peroxiredoxin Tsa1 in *Saccharomyces cerevisiae*. *Mol Cell, 43*(5), 823-833. doi:10.1016/j.molcel.2011.07.027

Neumann, C. A., Krause, D. S., Carman, C. V., Das, S., Dubey, D. P., Abraham, J. L., . . . Van Etten, R. A. (2003). Essential role for the peroxiredoxin Prdx1 in erythrocyte antioxidant defence and tumour suppression. *Nature, 424*(6948), 561-565.

Noichri, Y., Palais, G., Ruby, V., D'Autreaux, B., Delaunay-Moisan, A., Nystrom, T., . . . Toledano, M. B. (2015). In vivo parameters influencing 2-Cys Prx oligomerization: The role of enzyme sulfinylation. *Redox Biol, 6*, 326-333. doi:10.1016/j.redox.2015.08.011

Nystrom, T., Yang, J., & Molin, M. (2012). Peroxiredoxins, gerontogenes linking aging to genome instability and cancer. *Genes Dev, 26*(18), 2001-2008. doi:10.1101/gad.200006.112

Olahova, M., & Veal, E. A. (2015). A peroxiredoxin, PRDX-2, is required for insulin secretion and insulin/IIS-dependent regulation of stress resistance and longevity. *Aging Cell, 14*(4), 558-568. doi:10.1111/acel.12321

Parrinello, M., & Rahman, A. (1981). Polymorphic Transitions in Single-Crystals - a New Molecular-Dynamics Method. *Journal of Applied Physics, 52*(12), 7182-7190. doi:Doi 10.1063/1.328693

Peeters, K., Van Leemputte, F., Fischer, B., Bonini, B. M., Quezada, H., Tsytlonok, M., . . . Thevelein, J. M. (2017). Fructose-1,6-bisphosphate couples glycolytic flux to activation of Ras. *Nat Commun, 8*(1), 922. doi:10.1038/s41467-017-01019-z

Ponder, J. W., & Case, D. A. (2003). Force fields for protein simulations. *Adv Protein Chem, 66*, 27-85.

Rappsilber, J., Mann, M., & Ishihama, Y. (2007). Protocol for micro-purification, enrichment, pre-fractionation and storage of peptides for proteomics using StageTips. *Nat Protoc, 2*(8), 1896-1906. doi:10.1038/nprot.2007.261

Reiter, W., Anrather, D., Dohnal, I., Pichler, P., Veis, J., Grotli, M., . . . Ammerer, G. (2012). Validation of regulated protein phosphorylation events in yeast by quantitative mass spectrometry analysis of purified proteins. *Proteomics, 12*(19-20), 3030-3043. doi:10.1002/pmic.201200185

Santangelo, G. M. (2006). Glucose signaling in *Saccharomyces cerevisiae*. *Microbiol Mol Biol Rev, 70*(1), 253-282.

Schulz, T. J., Zarse, K., Voigt, A., Urban, N., Birringer, M., & Ristow, M. (2007). Glucose restriction extends Caenorhabditis elegans life span by inducing mitochondrial respiration and increasing oxidative stress. *Cell metabolism, 6*(4), 280-293. doi:10.1016/j.cmet.2007.08.011

Sjölander, J. J., Tarczykowska, A., Cossio, I., Redwan, N., Corap, S., Gao, C., . . . Sunnerhagen, P. (2020). Enhanced MAPK peroxide signalling by a small molecule protecting fission yeast MAPKK Wis1 from inhibitory thiol oxidation. *Mol Cell Biol, 40*(7), e00346-00319. doi:10.1128/MCB.00346-19

Smith, A., Ward, M. P., & Garrett, S. (1998). Yeast PKA represses Msn2p/Msn4p-dependent gene expression to regulate growth, stress response and glycogen accumulation. *Embo J, 17*(13), 3556-3564.

Sohal, R. S., & Forster, M. J. (2014). Caloric restriction and the aging process: a critique. *Free Radic Biol Med, 73*, 366-382. doi:10.1016/j.freeradbiomed.2014.05.015

Stocker, S., Maurer, M., Ruppert, T., & Dick, T. P. (2018). A role for 2-Cys peroxiredoxins in facilitating cytosolic protein thiol oxidation. *Nature chemical biology, 14*(2), 148-155. doi:10.1038/nchembio.2536

Stocker, S., Van Laer, K., Mijuskovic, A., & Dick, T. P. (2017). The Conundrum of Hydrogen Peroxide Signaling and the Emerging Role of Peroxiredoxins as Redox Relay Hubs. *Antioxid Redox Signal*. doi:10.1089/ars.2017.7162

Tagwerker, C., Flick, K., Cui, M., Guerrero, C., Dou, Y., Auer, B., . . . Kaiser, P. (2006). A tandem affinity tag for two-step purification under fully denaturing conditions: application in ubiquitin profiling and protein complex identification combined with in vivocross-linking. *Mol Cell Proteomics, 5*(4), 737-748. doi:10.1074/mcp.M500368-MCP200

Toda, T., Uno, I., Ishikawa, T., Powers, S., Kataoka, T., Broek, D., . . . Wigler, M. (1985). In yeast, RAS proteins are controlling elements of adenylate cyclase. *Cell, 40*(1), 27-36.

Truong, T. H., & Carroll, K. S. (2012). Bioorthogonal Chemical Reporters for Analyzing Protein Sulfenylation in Cells. *Current Protocols in Chemical Biology, 4*(2), 101-122. doi:10.1002/9780470559277.ch110219

Wilson, R. B., & Tatchell, K. (1988). SRA5 encodes the low-Km cyclic AMP phosphodiesterase of Saccharomyces cerevisiae. *Mol Cell Biol, 8*(1), 505-510.

Vizcaino, J. A., Csordas, A., del-Toro, N., Dianes, J. A., Griss, J., Lavidas, I., . . . Hermjakob, H. (2016). 2016 update of the PRIDE database and its related tools. *Nucleic Acids Res, 44*(D1), D447-456. doi:10.1093/nar/gkv1145

Woo, H. A., Yim, S. H., Shin, D. H., Kang, D., Yu, D. Y., & Rhee, S. G. (2010). Inactivation of peroxiredoxin I by phosphorylation allows localized H(2)O(2) accumulation for cell signaling. *Cell, 140*(4), 517-528. doi:10.1016/j.cell.2010.01.009

Yang, J., Gupta, V., Tallman, K. A., Porter, N. A., Carroll, K. S., & Liebler, D. C. (2015). Global, in situ, site-specific analysis of protein S-sulfenylation. *Nat Protoc, 10*(7), 1022-1037. doi:10.1038/nprot.2015.062

Yao, Y., Tsuchiyama, S., Yang, C., Bulteau, A. L., He, C., Robison, B., . . . Schmidt, M. (2015). Proteasomes, Sir2, and Hxk2 form an interconnected aging network that impinges on the AMPK/Snf1-regulated transcriptional repressor Mig1. *PLoS Genet, 11*(1), e1004968. doi:10.1371/journal.pgen.1004968

Zhang, J., Ye, Z. W., Singh, S., Townsend, D. M., & Tew, K. D. (2018). An evolving understanding of the S-glutathionylation cycle in pathways of redox regulation. *Free Radic Biol Med, 120*, 204-216. doi:10.1016/j.freeradbiomed.2018.03.038

Zhang, N., Quan, Z., Rash, B., & Oliver, S. G. (2013). Synergistic effects of TOR and proteasome pathways on the yeast transcriptome and cell growth. *Open Biol, 3*(5), 120137. doi:10.1098/rsob.120137

Zhang, P., Smith-Nguyen, E. V., Keshwani, M. M., Deal, M. S., Kornev, A. P., & Taylor, S. S. (2012). Structure and allostery of the PKA RIIbeta tetrameric holoenzyme. *Science, 335*(6069), 712-716. doi:10.1126/science.1213979

Zhu, K., Borrelli, K. W., Greenwood, J. R., Day, T., Abel, R., Farid, R. S., & Harder, E. (2014). Docking covalent inhibitors: a parameter free approach to pose prediction and scoring. *J Chem Inf Model, 54*(7), 1932-1940. doi:10.1021/ci500118s

Materials and methods

Strains and growth conditions

Yeast strains and plasmids are listed in Supplementary file 1 (Key resources table). The strains used in this study are derivatives of BY4741/BY4742. Strains were grown at 30°C in YPD 2% glucose (w/v) or in Yeast Nitrogen Base defined medium containing 2% glucose and complete supplement mixture (CSM) lacking the appropriate amino acids (Formedium) as described previously (Molin et al., 2011). To check the segregation of deletion markers in tetrad dissections YPD medium supplied with the following chemicals was used to check segregation of the dominant markers: *kanMX4* (G418 200 µg/ml), *natMX4* (ClonNAT 100 µg/ml), *hphMX4* (Hygromycin B 300 µg/ml), *bleMX4* (Phleomycin 40 µg/ml). To counterselect the p*TPK1-URA3* plasmid cells were grown in defined glucose CSM –HIS, 5-FOA medium containing YNB, glucose and CSM –URA, HIS; 50 mg/l uracil and 1 g/l 5-fluoroorotic acid.

Strain and plasmid constructions

Strains YMM170 (*ras2*Δ*tsa1*Δ*)* and YMM172 (*pde2*Δ*tsa1*Δ*)* were constructed by crossing strain YMM114 to BY4741 *ras2*Δ*::kanMX4* and BY4741 *pde2*Δ*::kanMX4* [Research Genetics, (Giaever et al., 2002)], respectively, and selecting for Mat alpha, methionine prototrophic, lysine auxotrophic, G418 resistant and nourseothricin resistant progeny. Strains YMM171 and YMM173 were constructed by crossing a BY4741 *pde2*Δ*::hphMX4* {*pde2*Δ*::kanMX4* from the deletion collection [Research Genetics, (Giaever et al., 2002)] marker-switched (Goldstein & McCusker, 1999) to *pde2*Δ*::hphMX4* to strain YMM170 (*ras2*Δ*tsa1*Δ) and selecting for Mat alpha, methionine prototrophic, lysine auxotrophic, G418 resistant, hygromycin resistant and nourseothricin sensitive (YMM171 *ras2*Δ*pde2*Δ) or nourseothricin resistant (YMM173 *ras2*Δ*pde2*Δ*tsa1*Δ) progeny. Strains YMM174 (*msn2*Δ*msn4*Δ), YMM175 (*pde2*Δ) and YMM176 (*pde2*Δ o/e *TSA1*) were constructed by crossing BY4741 *msn2*Δ*msn4*Δ (Caballero et al., 2011) or BY4741 *pde2*Δ*::kanMX4* [Research Genetics, (Giaever et al., 2002)] to strains YMM130 or BY4742 *his3*Δ*1::pRS403-Myc-TSA1*, respectively and selecting for Mat alpha, methionine prototrophic, lysine auxotrophic, histidine auxotrophic, hygromycin- and nourseothricin-resistant progeny (YMM174) or Mat alpha, methionine prototrophic, lysine auxotrophic, G418 resistant and histidine prototrophic progeny (YMM174 and YMM175). Strain YMM177 was constructed by marker-switching (Goldstein & McCusker, 1999) a Mat a *ras1*Δ*::kanMX4* spore, obtained from crossing strain BY4741 *ras1*Δ*::kanMX4* [Research Genetics, (Giaever et al., 2002)] to strain YMM114 and selecting for Mat a, methionine prototrophic, lysine auxotrophic and G418 resistant progeny, to *ras1*Δ*::hphMX4*. Strain YMM178 (*tpk1*Δ*/TPK1 tpk2*Δ*/TPK2 tpk3*Δ*/TPK3*) was constructed by crossing a BY4742 *tpk1*Δ*::kanMX4 tpk2*Δ*::natMX4* strain to a BY4741 *tpk3*Δ*::hphMX4* strain {*tpk3*Δ*::kanMX4* from the deletion collection [Research Genetics, (Giaever et al., 2002)] marker-switched (Goldstein and McCusker, 1999) to *tpk3*Δ*::hphMX4* resulting in a *tpk1Δ/TPK1 tpk2Δ/TPK2 tpk3Δ/TPK3* heterozygous diploid strain. A Mat alpha, G418- and hygromycin-resistant spore constitutes strain YMM179 whereas a Mat alpha, nourseothricin- and hygromycin-resistant spore constitutes strain YMM180. The BY4742 *tpk1*Δ*::kanMX4 tpk2*Δ*::natMX4* strain was constructed by introducing *tpk2*Δ*::natMX4* PCR amplified from a BY4742 *tpk2*Δ*::natMX4* strain (Costanzo et al., 2010) into strain BY4741 *tpk1*Δ*::kanMX4* [Research Genetics, (Giaever et al., 2002)] selecting for nourseothricin- and G418-resistance and verifying the deletion by diagnostic PCR. A BY4742 *tpk1*Δ*tpk2*Δ*tpk3*Δ p*TPK1-URA3* haploid strain (YMM181) was constructed by transforming strain YMM177 with plasmid p*TPK1-URA3* and sporulating the strain selecting for a Mat alpha methionine prototrophic, lysine auxotrophic, G418-, nourseothricin-, hygromycin B-resistant and uracil auxotrophic progeny. Strains YMM182-YMM186 were constructed by transforming strain YMM180 with plasmids pRS313 (YMM181), pRS313-*TPK1*

(YMM183), pRS313-*tpk1C243A* (YMM184) and pRS313-*tpk1C243D* (YMM185) and pRS313-*tpk1T241A* (YMM186). Counterselecting p*TPK1-URA3* on 5-FOA medium resulted in strains YMM187 (BY4742 *tpk1*Δ*tpk2*Δ*tpk3*Δ pRS313-*TPK1*), YMM188 (BY4742 *tpk1*Δ*tpk2*Δ*tpk3*Δ pRS313-*tpk1C243A*), YMM189 (BY4742 *tpk1*Δ*tpk2*Δ*tpk3*Δ pRS313-*tpk1C243D*) and yMM190 (BY4742 *tpk1*Δ*tpk2*Δ*tpk3*Δ pRS313-*tpk1T241A*), respectively. Strain YMM191 (*ras2*Δ*trx1*Δ*trx2*Δ) was constructed by crossing strain YMM113 (*ras2*Δ) to strain YMM143 (*trx1*Δ*trx2*Δ) selecting for Mat alpha, methionine prototrophic, lysine auxotrophic, G418-, nourseothricin- and hygromycin B-resistant progeny. Strain YMM192 was constructed by marker-switching strain BY4741 *tsa1*Δ*::kanMX4* [Research Genetics, (Giaever et al., 2002)] into BY4741 *tsa1*Δ*::bleMX4* using a bleMX4 cassette PCR amplified from plasmid pUG66 (Gueldener, Heinisch, Koehler, Voss, & Hegemann, 2002) using primers PR78 and PR79 (Goldstein & McCusker, 1999). Strain yMM193 was constructed by crossing strains yMM180 and yMM192 selecting for a Mat a, nourseothricin+, hygromycin+ and phleomycin+ spore. Strain WR1832 was constructed by first introducing PCR amplified *trp1Δ::kanMX4* DNA (Longtine et al., 1998) into strain YMM180, verification of cassette integration by PCR and loss of the ability to grow without tryptophan supplement and next by *HBH::TRP1* C-terminal tagging of *TPK1* and PCR based verification as described (Tagwerker et al., 2006). Strains yCP101-yCP104 were constructed by crossing Mat a *his3Δ1::pRS403* or *his3Δ1::pRS403-myc-TSA1* spores, obtained in crosses generating strains yMM175 above, either to strain yMM183 or to strain yMM187 also carrying plasmid *pRS316-tpk1C243A*. Methionine prototrophic, lysine auxotrophic, histidine prototrophic, 5-FOA-sensitive, G418+, nourseothricin+ and hygromycin B+ progeny obtained in these crosses constitute strains yCP101-yCP104 listed in Table S1. Strains yCP105 and yCP106 were constructed by crossing strains yMM187 (p*TPK1*) or yMM189 (p*tpk1T241A*), respectively, to strain yMM192 selecting for Mat alpha, Met+, Lys-, G418+, Nat+, Hyg+, Phleomycin+, His+ progeny. Strain yCP107 was constructed by crossing strain WR1832 to yMM193 and selecting for Mat alpha, Met+, Lys-, G418+, Nat+, Hyg+, Phleomycin+, Trp+ progeny.

Plasmids pRS313-*tpk1C243A*, pRS313-*tpk1C243D*, pRS313-*tpk1T241A* and pRS316-*tpk1C243A*, were constructed by site directed mutagenesis of the pRS313-*TPK1* or pRS316-*TPK1* plasmids (Eurofins Genomics). Plasmids pRS315-*trx1C34S*-ProtA and pRS315-*trx2C31SC34S*-ProtA were constructed by site-directed mutagenesis of plasmid pRS315-*TRX2*-ProtA (GenScript). The correct sequence of all plasmids constructed was verified by sequencing.

Lifespan Analyses

Lifespan analyses were performed as previously described by counting the number of daughters produced in a cohort of mother cells (Erjavec et al., 2007).

2D-PAGE

Protein synthesis rates of the indicated proteins were determined in ^{35}S-Methionine labelled protein extracts separated by two-dimensional polyacrylamide gel electrophoresis as described (Maillet et al., 1996; Molin et al., 2011). Tsa1 sulfinylation was determined by comparing levels of sulfinylated Tsa1 (Tsa1-SOOH) to non-sulfinylated Tsa1 on silver-stained 2D gels as described (Molin et al., 2011).

Spot tests

H_2O_2 resistance was tested with mid-exponential-phase (A_{600}=0.3, 3 × 10^6 cells/ml) cells that were diluted (x5, x50, x500, x5000, x50000) and spotted onto SD media containing 0 to 1 mM H_2O_2 or YPD media containing 0 to 2 mM. The number of colonies after 2 days incubation at 30 ◦C on H_2O_2 plates was divided with the number on control plates to get H_2O_2-resistance (%).

For glycogen accumulation, plates incubated for 2 days at 30 ◦C were exposed to iodine-bead fumes for 2.5 min and scanned immediately.

Spore viability

The viability of spores segregating in the sporulation and dissection of a heterozygous diploid *ras1*Δ*::hphMX4/RAS1 ras2*Δ*::kanMX4/RAS2 tsa1*Δ*::natMX4/TSA1* strain obtained by crossing strain YMM176 (*ras1*Δ*::hphMX4*) to strain YMM170 (BY4742 *ras2*Δ*::kanMX4 tsa1*Δ*::natMX4*) was analyzed after 4 days of incubation at 30°C in 32 tetrads where 1) all markers analyzed (*hphMX4, kanMX4, natMX4, MET15, LYS2*) segregated 2:2, 2) the exact genotypes of all spores were possible to deduce from this information and 3) the genotypes of dead spores were assigned based on markers present in the other spores dissected from the same tetrads. Similarly, spore viability of spores segregating in a heterozygous diploid *tpk1*Δ*::kanMX4/TPK1 tpk2*Δ*::natMX4/TPK2 tpk3*Δ*::hphMX4/TPK3 tsa1*Δ*::bleMX4/TSA1*, obtained by crossing strain YMM191 (BY4741 *tsa1*Δ*::bleMX4*) to strain YMM186 (BY4742 *tpk1*Δ*::kanMX4 tpk2*Δ*::natMX4 tpk3*Δ*::hphMX4* expressing pRS313-*TPK1*), was analyzed in 43 tetrads where all chromosomal markers analyzed (*kanMX4, natMX4, hphMX4, bleMX4, MET15, LYS2*) segregated 2:2. The ability to grow in the absence of histidine supplementation (-HIS) was taken as an indication that the pRS313-*TPK1* plasmid was present.

Quantitative Real-Time PCR Analysis

Cell cultures were harvested in mid-exponential phase and resuspended in 1 ml Trizol Reagent (Invitrogen) and homogenized with silica beads by Fast prep (6.5 m/s, 30 sec, interval 2.5min, 4 ◦C). RNA was extracted using phenol chloroform extraction and precipitated with sodium acetate/ethanol. The pellet was treated with DNase for 30min followed by heat-inactivation of the enzyme. The RNA was purified with Invitrogen PureLink RNA Mini Kit columns and converted to cDNA following the QIAGEN QuantiTect Reverse Transcription Kit. Q-PCR was performed with 50ng cDNA by using BioRad iQ SYBR Green Supermix and quantified with the BioRad iCycler, iQ5. Relative levels of mRNA were calculated by using cycle times of *ACT1* as a reference gene.

Quantitative analyses of Msn2-GFP localization

Msn2-signaling was analyzed as described previously (Bodvard et al., 2017). Briefly, the fraction of cells displaying nuclear localization of Msn2-GFP (nucleus/cytoplasm signal ratio >1.28) at each time point was calculated and used to calculate the total time Msn2 spent in the nucleus during a 60 min experiment.

Measurement of Ras2-GTP *in vivo*

Ras2-GTP level were measured as a ratio between Ras2-GTP and total Ras2 as described previously (Colombo & Martegani, 2014; Peeters et al., 2017). Mid-exponential phase yeast cells were harvested and lysed with glass- beads in Fast-prep (6.0 m/s, 20sec, interval 2.5 min) in lysis buffer [50 mM Tris-HCl, 200 mM NaCl, 2.5 mM $MgCl_2$, 10% glycerol, 1% Triton X100, cOmplete Protease inhibitor EDTA-free]. The supernatant with 1.5mg of total protein was incubated with a bed volume 50 µL of glutathione S-transferase (GST)-RBD fusion protein pre-bound to glutathione-Sepharose for 1 h at 4 °C and washed three times with lysis buffer by centrifugation. For elution the beads were boiled for 5 min at 98 ◦C in SDS-sample buffer (6% SDS, 62.5 mM Tris-HCl pH 8.7, 30% Glycerol, 0.75% β-mercaptoethanol). Through western blotting, Ras2-GTP and total Ras2 proteins were detected with anti-Ras2 antibodies. Determination of ratios between Ras2-GTP and total Ras2 was performed by ImageJ.

cAMP measurement

cAMP measurements were performed as previously described (Caballero et al., 2011; Parts et al., 2011). 2×10^8 cells grown to midexponential phase were pelleted, washed, and resuspended in 1 ml cold milliQ water. Metabolites were extracted by adding 1.2 ml TCA (0.5 M) and occasional vigourous vortexing while samples were kept on ice for 15 min. TCA was removed by ether extraction. cAMP levels were determined by the LANCE cAMP 384 kit in 40 µL total reactions and by comparing to the standards supplied. The values for cAMP were normalized to the wild type level.

Global H_2O_2 scavenging in the medium

Medium peroxide determinations were performed using a ferrithiocyanate spectrophotometric assay (Molin et al., 2007). After bolus addition of H_2O_2, 100 µL sample aliquots were withdrawn and cultures were arrested by the addition of 1 ml ice-cold 10% TCA. After pelleting cells 180 mM KSCN and 1.4 mM $Fe(NH_4)_2(SO_4)_2$ final concentrations were added to the supernatants. Absorbance at 480 nm was subsequently determined and compared to equally TCA-treated H_2O_2 standards diluted in medium.

Isolation of old cells

Old cells were obtained as previously described by sorting biotin-labeled mother cells using the MagnaBind streptavidin system (Sinclair and Guarente, 1997). Briefly, mid-exponential phase cells were labeled with EZ-Link Sulfo-NHS-LC Biotin and grown overnight in minimal media (CSM-His). The cells were incubated with streptavidin-conjugated magnetic beads for 2 h and then sorted magnetically with the unlabeled cells being washed away. Sorted cells were then grown overnight and the streptavidin labeling procedure was repeated before sorting one last time. After sorting the cells were incubated for 1 h in CSM-His media at 30 ◦C for recovery before microscopy.

Measurements of cytoplasmic H_2O_2 using HyPer3

Fluorescence of the ratiometric probe HyPer-3 (Bilan et al., 2013) was acquired using an Olympus IX81 motorized microscope with a PlanApoN 60x/1.42 Oil objective and a 12-bit Hamamatsu camera. Shifts in the fluorescence intensities were acquired with excitation around 500 nm (485/20 nm) and 420 nm (427/10 nm filter) and an emission filter around 520 nm (Fura 2 filter). For bolus addition of H_2O_2, cells in midexponential phase were incubated with 0.2 mM H_2O_2 for 10 min and immediately imaged.

Image analysis of HyPer3 fluorescence

Image and signal analysis was performed using the MATLAB toolbox 2016b. Cell segmentation is performed with the CellX algorithm using the bright-field channel. The fluorescent intensity data was obtained from fluorescent images and data is presented as the median 500 nm fluorescent signal normalized to the median fluorescent 420 nm signal by dividing the latter with the former.

AKAR4 FRET-based PKA activity measurements

Detection of cyan fluorescent protein CFP to yellow fluorescent protein YFP FRET in the AKAR4 sensor was performed as described previously (Depry & Zhang, 2011; Molin et al., 2020). CFP was excited at 427/10 nm, YFP was excited at 504/6 nm and emission was monitored using a Semrock dual bandpass filter (part no: FF01-464/547). Images were acquired using an automated epi-fluorescence microscope (Olympus IX81) equipped with a × 60 oil-immersion objective (numerical aperture 1.4, PlanApoN × 60/1.42 Oil, Olympus) and an electron-multiplying charge-coupled device camera (12-bit Hamamatsu camera). The yeast cells were kept in a heated perfusion chamber (FCS2, Bioptechs Inc.) at 28 °C to avoid heat-induced stress responses. The objective was heated to 26.2 °C (according to the manufacturer's instructions) to maintain a stable temperature in the perfusion chamber. The

cover glasses were precoated for 1.5 h with protein concanavalin A, 0.5 µg µl−1 in 0.01 M PBS, to immobilize yeast cells on the surface

Immunoprecipitation

Cells from 50 mL/sample of mid-exponential phase YPD culture was pelleted, the pellet was washed with cold water and pelleted again, washed with 1 mL lysis buffer (50 mM Tris HCl pH 8.0, 150 mM NaCl, 1 mM EDTA, 10% Glycerol, 5 mM $MgCl_2$ and protease-inhibitor cocktail). Cells were broken in 0.35 mL lysis buffer by beads at 4 degrees in a Fastprep FP120 cell disrupter (Bio101/ThermoSavant, speed 5 m/sec, 4 times 40 seconds with > 1 min on ice in between each agitation). The extract was pelleted at 12500 rpm at 4 degrees and the supernatant was used for subsequent analyses. An aliquot of supernatant was withdrawn for analysis of input protein levels (load sample). Beads were prewashed with lysis-buffer (100 uL) before incubated with protein extract (300 uL at 1ug/uL) at 4 degrees overnight. Beads were pelleted by centrifugation at 1000 rpm, 1 min, washed 3 times with lysis buffer and boiled at 95ºC, 5 min with Laemmli buffer (IP sample). 10 uL of each sample was separated on an SDS-PAGE gel for 1.5 h at 120V an blotted as described below. Membranes were incubated overnight with the primary antibody at 4 degrees.

Immunoblot analysis

Immunoblot analysis of selected proteins was performed as described previously (Biteau, Labarre, & Toledano, 2003; Molin et al., 2011). Prior to separation on 12% Bis-Tris NuPAGE gels using an XCell SureLock MiniCell (Invitrogen) in NuPAGE MOPS running buffer as recommended by the supplier protein extracts were heated in Laemlii buffer (pH 8.7) either in the presence of β-mercaptoethanol (5%, reducing) or not (non-reducing) as indicated. Transfer to Immobilon-FL PVDF membranes was done using an XCell II Blot Module kit. Membranes were analyzed by the Odyssey infrared imaging system (LI-COR biosciences) as recommended by the suppliers.

Glutathionylation of Tpk1 was assayed using anti-glutathione immunoblot on Tpk1-HB immunoprecipitated by Ni^{2+}-Sepharose beads following a simplified protocol similar to that used during MS sample preparation (see below). We verified that the anti-glutathione immunoblot signal in Tpk1 completely disappeared upon extract reduction by β-mercaptoethanol.

Growth conditions for MS analysis

Cells were grown at 30°C in yeast extract/peptone (YP) medium, containing 2% glucose as carbon source. Three independent experimental replicates were performed for each experimental condition. For each replicate, we inoculated 750ml YPD cultures, which were incubated (with shaking) overnight until OD600 = 1. Oxidative stress was induced by adding 0.4 mM or 0.8 mM (final concentration) H_2O_2 for 10 minutes.

Mass spectrometric sample preparation

HB (poly histidine, biotinylation signal) tandem affinity purifications were performed as described elsewhere (Reiter et al., 2012). Cells were harvested by filtration and immediately deep-frozen in liquid N_2. Cells were grinded using a SPEX Freezer Mill 6870 (SPEXSamplePrep, Metuchen, NJ, USA) with the following settings: 7 cycles: 3 min breakage (15 CPS), 3 min cooling, resuspended in buffer 1 (6 M guanidine HCl, 50 mM Tris pH8.0, 5 mM NaF, 1 mM PMSF, 0.1% Tween, cOmplete Protease inhibitor cocktail, pH 8) and cleared of debris by centrifugation 13.500 x g, 15 min, 4°C. Cleared extracts were incubated (4 hours, room temperature) with Ni^{2+}-Sepharose beads, washed with urea buffer (8M urea,

50mM sodium phosphate buffer pH8.0, 300mM NaCl, 0.1% Tween20) and urea buffer pH 6.3. Proteins were eluted in urea buffer pH 4.3 containing 10mM EDTA, incubated overnight with streptavidin-agarose beads, washed using urea wash buffer containing 1% SDS and urea wash buffer without SDS. Beads were washed five times with 50 mM ammonium bicarbonate (ABC). Cys-residues were alkylated with IAA (25% w/w of the estimated amount of protein). Excess IAA was washed out by ABC. Proteins were digested with 300 ng trypsin at 37°C overnight. Digestion was stopped with trifluoroacetic acid (0.5% final concentration) and the peptides were desalted using C18 Stagetips (Rappsilber, Mann, & Ishihama, 2007). 50 fmol of the Peptide Retention Time Calibration Mixture was spiked in each sample for quality control.

Mass spectrometry analysis of Tpk1

Peptides were separated on an Ultimate 3000 RSLC nano-flow chromatography system (Thermo-Fisher), using a pre-column (Acclaim PepMap C_{18}, 2 cm × 0.1 mm, 5 µm, Thermo-Fisher), and a C_{18} analytical column (Acclaim PepMap C18, 50 cm × 0.75 mm, 2 µm, Thermo-Fisher). A segmented linear gradient from 2% to 35% solvent B (solvent B: 80% acetonitrile, 0.1% formic acid; solvent A: 0.1% formic acid) was applied at a flow rate of 230 nL/min over 120 min. A Proxeon nanospray flex ion source (Thermo Fisher) using coated emitter tips (New Objective) was used for ionization. The capillary temperature was set to 200°C. Peptides were analyzed on an Orbitrap Fusion Lumos Tribrid mass spectrometer (Thermo Fisher). The mass spectrometer was operated in data-dependent mode, survey scans were obtained in a mass range of 380-1500 m/z with lock mass activated, at a resolution of 120,000 at 200 m/z and an automatic gain control (AGC) target value of 4E5. The maximum cycle time was set to 2.5 s and the most abundant precursors were selected for fragmentation by high-energy collision at 30% collision energy. Fragmented precursors were excluded from further fragmentation for 30s (with +/- 5 ppm accuracy) and peptides with charge +1 or > +6 were excluded from MS/MS analysis. The most abundant Tpk1 Cys containing peptide forms have been added to an inclusion list as specified in the raw files. MS proteomics data have been deposited to the ProteomeXchange Consortium through the Proteomics Identifications database (PRIDE) partner repository (Vizcaino et al., 2016) with the data set identifiers PXD012617.

Closed database search

Peptide identification and label free quantification (LFQ) were performed using MaxQuant (version 1.6.0.16) with default parameters. *Saccharomyces cerevisiae* reference proteome database (UniProt, version January 2017) in combination with a common laboratory contaminants database (MQ) was used for peptide spectrum matching. N-terminal acetylation, deamidation of asparagine and glutamine, oxidation of methionine, tri-oxidation and glutathionylation of cysteine and phosphorylation of serine, threonine and tyrosine were set as variable protein modification. Carbamidomethylation of cysteine was set as fixed. A maximum of 5 variable modifications per peptide was allowed. Leucine and isoleucine were treated as indistinguishable. Enzyme specificity was set to "Trypsin/P". A maximum of 2 missed cleavages per peptide was allowed. 'Requantify' and "Match between runs" was activated. MaxLFQ (implemented in the MaxQuant package) was used for MS1-based label free quantification and normalization of protein groups.

Open search analysis of selected peptides

To screen for protein modifications in an unbiased manner we initially performed an open search using MSFragger in FragPipe (Kong, Leprevost, Avtonomov, Mellacheruvu, & Nesvizhskii, 2017). The default open search parameters were used, with trypsin specificity, +/- 500 Da windows and oxidation

of methionine and carbamidomethylation of cysteine as variable modifications. The observed mass shifts were inspected and filtered for the most abundant and relevant modifications occurring in Tpk1.

Targeted mass-spectrometry

Parallel-Reaction-Monitoring (PRM) assays were generated based on the peptide information obtained by MaxQuant. We selected Tpk1 and Tsa1 peptides for targeted relative LFQ as specified in Expanded View tables XY, datasheets 4 to 6.Peptides were separated using a 120 min gradient (HPLC setup as described above). PRM data acquisition was performed using a scheduled method with 20 min windows for each target based on the retention time determined in the shotgun-approach. Raw data were obtained on an Orbitrap Q Exactive HF-X (Thermo Fisher Scientific) mass spectrometer applying the following settings: survey scan with 60k resolution, AGC 1E6, 60 ms IT, over a range of 400 to 1400 m/z, PRM scan with 30 k resolution, AGC 1E5, 200 ms IT, isolation window of 1.0 m/z with 0.3 m/z offset, and NCE of 27%.

Wash runs were checked for potential peptide carry-over in between samples using same HPLC and MS methods. Data analysis, manual validation of all transitions (based on retention time, relative ion intensities, and mass accuracy), and relative quantification was performed in Skyline. Up to six characteristic transitions were selected for each peptide and their peak areas were summed for peptide quantification (total peak area). MS1 signals of PRTC standards were used as global standards for normalization in Skyline to account for fluctuations in instrument performance. The mean of the log2 Tpk1 non-modified peptide intensities was used to normalize Tpk1 modified peptides and Tsa1 peptides to account for differences in Tpk1 levels. Tsa1 peptide intensities (anti-log) were summed up to obtain values for relative protein abundance.

Cysteine sulfenylation assay by DYn-2 labeling, protein extraction and click chemistry

Mid-exponential cells (10 ml at OD_{600}=0.5) were treated with of DYn-2 (0.5 mM) for 30 min, at 30 °C and cell suspensions were next exposed to 0.5 mM H_2O_2 for 5 min. To the cultures trichloroacetic acid (TCA) was added to a final concentration of 20 %, followed by centrifugation (6000 x g, 5 min, 4°C) and pellets were lysed with glass beads (equivalent of 0.1 ml of beads) in 0.2 ml of TCA (20 %). Lysates were centirfuged (14000 x g, 15 min, 4°C) and pellets were washed twice with acetone, dried and solubilized in 0.2 ml Hepes (100 mM) buffer containing cOmplete™ mini EDTA-free protease inhibitor cocktail (Roche) (1 tablet/20 ml of buffer solution), 25 µg/ml phenylmethylsulfonylfluoride, 0.1% Nonidet P-40, 2% SDS, pH 7.4. Protein content was determined using a standard DC Protein Assay (Bio-Rad). A copper (I)-catalyzed azide-alkyne cycloaddition (CuAAC) click chemistry reaction was performed on 0.2 mg of protein as previously described (Truong & Carroll, 2012; Yang et al., 2015). Briefly, cyanine5 azide (0.5 mM), copper(II)-TBTA complex (1 mM) and ascorbate (2 mM) were added to the lysates, protected from light and incubated for 1 h at room temperature under rotation. The CuAAC reaction was quenched by adding EDTA (1 mM) for 10 min. The solution was precipitated by methanol/chloroform precipitation (sample/methanol/chloroform, 4/4/1 (v/v/v)) and centrifuged (14000 x g, 15 min, 4°C). The protein pellet obtained were between the organic and aqueous layers, both layers were aspirated. A solution of methanol/chloroform (H_2O/methanol/chloroform, 4/4/1 (v/v/v) was added to the protein pellet and centrifuged (14000 x g, 15 min, 4°C). Both layers were aspirated and the obtained pellet was subsequently washed twice with methanol. Protein pellets were resuspended in 100 mM Hepes buffer containing 2% SDS. Biotinylated proteins were enriched with Pierce™ streptavidin bead (Thermo Scientific™). The protein pellets were mixed to a pre-washed streptavidin beads (100 mM Hepes buffer). The samples were incubated for 2h at room temperature and subsequently washed twice with 1% SDS, twice with 4M urea, once with 1M NaCl and twice with PBS. After each wash step,

beads were collected by centrifugation. Beads were finally resuspended in 5X Laemmli buffer and boiled for 5 min at 95 °C. Samples were resolved by SDS-PAGE and analyzed for fluorescence at 700 nm (Cyanine5) on an Odyssey CLx (Licor).

Homology modeling

A model of the yeast PKA tetramer structure was obtained by homology modeling. The protein sequences of yeast Tpk1 (catalytic subunit of PKA) and Bcy1 (regulatory subunit of PKA) were obtained from Genbank (ID: 1023942850 and ID: 1023943330, respectively). The crystal structure of mouse PKA (PDBID: 3TNP) was used as the template for the homology calculations. The catalytic and regulatory subunits of yeast PKA and mouse PKA shares 48% and 42% sequence similarity, respectively. The homology model was built using StructurePrediction panel (Jacobson, Friesner, Xiang, & Honig, 2002) in Schrödinger Suite (Schrödinger, LLC, New York, NY). The ClustralW method was used to align the target and template sequences in Prime, the energy-based was selected for model building method, and homo-multimer was selected for multi-template model type.

Covalent docking

Covalent docking was carried out to obtain a model for glutathionylated Tpk1. The Tpk1 crystal structure [PDB ID: 1FOT, (Mashhoon, Carmel, Pflugrath, & Kuret, 2001)] were prepared using the Protein Preparation utility in Schrodinger to assign the correct protonation state and fix the missing side chains and loops. The glutathione was built by 3D builder and prepared by LigPre utility in Schrodinger. The Covalent-Dock panel (Zhu et al., 2014) in Schrodinger was used to predict the pose of the glutathione attaching to Cys243. The reaction type was set to be disulfide formation, the docking mode was set to be thorough pose prediction, the other parameters were all set to be default. At the final step, Prime Energy was used to rank the poses of the ligand. Covalent docking was performed on dephosphorylated Tpk1 structure.

Molecular dynamics simulations

Molecular dynamics simulations were carried out to study structural changes of Tpk1 upon phosphorylation and glutathionylation. MD simulations non-modified Tpk1, Cys243 glutathionylation Tpk1, Thr241 phosphorylation Tpk1, Cys243 glutathionylation and Tpk1 phosphorylation co-existed Tpk1 were carried out. The GROMACS software (Abraham et al., 2015) was used for the MD simulations and the Amber 99 (Ponder & Case, 2003) force field was selected to assign the parameters for different amino acid residues. The glutathionylation and phosphorylation parameters was generated from Ambertools, and incorporated into the GROMACS software.

The systems were solvated with a buffer distance of 10.0 Å TIP3P water in periodic boxes, and then 0.1 mol/L of Na^+ and Cl^- ions were added to adjust the systems to electroneutrality condition. Then 200 steps of the steepest descent energy minimization was carried out to remove close contacts in the obtained systems. A 2ns position-restrained simulation with a constant pressure ensemble (NPT) was performed to make sure the water molecules would reach more favorable positions. The parameters for position-restrained simulation are set to be: a time step = 1 fs, temperature = 298 K, and coupling pressure = 1 bar, Coulomb cutoff = 10 Å, Lennard-Jones cutoff = 10 Å, particle-mesh Ewald summation (Darden, York, & Pedersen, 1993; Essmann et al., 1995) was used for longrange electrostics. The temperature and pressure was controlled by Berendsen coupling algorithm (Berendsen, Postma, Vangunsteren, Dinola, & Haak, 1984), with the time constants of 0.1 ps for temperature and 1.0 ps for pressure coupling. All bond lengths was contrained by the LINCS algorithm (Hess, Bekker, Berendsen, & Fraaije, 1997). Following the position-restrained simulation, 100 ns production simulations with NPT

ensemble were performed on each system for further study the protein conformational changes. In this step, the Nose–́ Hoover thermostat (Hoover, 1985), with a time constant 0.1 ps, was used to control the temperature and the Parrinello–Rahman barostat (Parrinello & Rahman, 1981), with a time constant 1.0 ps, was used to control the pressure. The other parameters were the same as those in the position-restrained simulations.

Quantification and statistical analysis

All experiments were repeated at least three times (biological replicates) to ensure reproducibility. Biological replicates of experiments were performed in separate, independent experiments (typically on a separate day). No data were excluded in averages/median values presented in figures. Details on the number of replicates and statistical analyses performed in relation to the specific figures are available below.

Figure 1. B) Lifespans were tested for statistical significance by the Mann-Whitney U test (www.socscistatistics.com/tests/mannwhitney/Default2.aspx). **B)** Lifespans of wt control and o/e *TSA1* strains are significantly different using the Mann Whitney U test (n=167 and 168 cells, p<0.00001). Lifespans of *pde2Δ* control and *pde2Δ* o/e *TSA1* strains are not significantly different (n=81 and 84, respectively, p=0.58). **D)** Hsp12 levels are significantly different between control and o/e *TSA1* strains (n=3, p=0.033) whereas Act1 levels are not (n=3, p=0.69). **E)** Lifespans of the wt (n=157) vs the *tsa1Δ* (n=293) and the *tsa1Δ* vs *ras2Δtsa1Δ* (n=283) are significantly different at p<0.00001. The lifespan of the *ras2Δ* (n=138) is not significantly different from the *ras2Δtsa1Δ* (p=0.276). **F)** Lifespans of the wt (n=157) vs the *pde2Δ* (n=120), the *ras2Δtsa1Δ* vs *ras2Δpde2Δtsa1Δ* (n=164) and the *tsa1Δ* (n=293) vs *pde2Δtsa1Δ* (n=242) are significantly different at p<0.00001. Lifespans of the *ras2Δpde2Δ* (n=124) vs *pde2Δ* are significantly different (p=0.00068) whereas the lifespans of *pde2Δ* vs *pde2Δtsa1Δ* are not significantly different (p=0.757).

Figure 2. A) Doubling times of wt and *ras2Δ* strains are significantly different at p=0.047 whereas the difference between the *tsa1Δ* and the *ras2Δtsa1Δ* is not statistically significant using a two-sided t-test assuming equal variance (p=0.77). **C)** Doubling times of control and mc-*IRA2* strains are significantly different for the wt (n=7 each, p=7.4 x 10^{-6}), the *tsa1ΔYF* (n=3 and 4, respectively, p=0.0032), *msn2Δmsn4Δ* (n=3 each, p=0.026) and *trx1Δtrx2Δ* (n=15 and 13, respectively, p=0.012). In none of the other strains are control and mc-*IRA2* different (*tsa1Δ* n=3 each, p=0.87; *tsa1C48S*, n=3 each, p=0.71; *tsa1C171S*, n=4 each, p=0.11; *tsa1ΔYFC171S*, n=4 each, p=0.77; *pde2Δ*, n=3 each, p=0.66. **D**) Relative *HSP12* levels were significantly different between wt control and mc-*IRA2* strains (n=15 and 9, respectively, p=1.0 x 10^{-14}), between wt mc-*IRA2* and *tsa1Δ* mc-*IRA2* strains (n=9 and 8, respectively, p=1.9 x 10^{-6}), between wt mc-*IRA2* and *tsa1C171S* mc-*IRA2* strains (n=9 and 4, respectively, p=0.026), between wt mc-*IRA2* and *tsa1ΔYFC171S* mc-*IRA2* strains (n=9 and 6, respectively, p=0.00083) and between wt mc-*IRA2* and *pde2Δ* mc-*IRA2* strains (n=9 and 6, respectively, p=4.8 x 10^{-8}). No significant difference was seen between wt mc-*IRA2* and *tsa1ΔYF* mc-*IRA2* strains (n=9 and 3, respectively, p=0.53). Relative *CTT1* levels were significantly different between wt control and mc-*IRA2* strains (n=24 and 21, respectively, p=3.4 x 10^{-13}), between wt mc-*IRA2* and *tsa1Δ* mc-*IRA2* strains (n=21 and 6, respectively, p=0.0073), between wt mc-*IRA2* and *tsa1C171S* mc-*IRA2* strains (n=9 and 4, respectively, p=0.026), between wt mc-*IRA2* and *tsa1ΔYF* mc-*IRA2* strains (n=21 and 3, respectively, p=0.027), between wt mc-*IRA2* and *tsa1ΔYFC171S* mc-*IRA2* strains (n=21 and 6, respectively, p= p=4.9 x 10^{-5}) and between wt mc-*IRA2* and *pde2Δ* mc-*IRA2* strains (n=21 and 6, respectively, p=3.5 x 10^{-7}). **F)** Doubling times of control and mc-*IRA2* strains are significantly different for the wt control (n=3 each, p=0.00042), the wt o/e *PDE2* (n=3 each, p=0.00091) and for the *tsa1Δ* mc-*PDE2* strain (n=3,

p=0.0058) but not for the *tsa1Δ* control strain (n=3 each, p=0.20). **G)** The time Msn2 spent in the nucleus is significantly different in the wt vector control (n=82) vs. *mc-BCY1* (n=76, p<0.001) but not *tsa1Δ* vector control (n=46) vs. *mc-BCY1* (n=74, p=0.14). **H)** Relative Ras2-GTP/total Ras values in the control and mc-*IRA2* are significantly different in a two tailed t-test with unequal variance for the wt (n=3, p=0.0041). Values for the *pde2Δ* control vs mc-*IRA2* (n=3, p=0.015) and the *tsa1Δ* control vs mc-*IRA2* (n=3, p=0.030) are significantly different in a two-tailed t-test with equal variance. **I)** cAMP levels are significantly different only between wt and *pde2Δ* strains (n=4 each, wt yEP24 vs pde2 yEP24, p=0.0050 and wt pKF56 vs pde2 pKF56, p=1.4 x 10^{-5}). No significant differences were seen between wt and *tsa1Δ* strains (n=4 each, wt yEP24 vs *tsa1Δ* yEP24, p=0.86 and wt pKF56 vs *tsa1Δ* pKF56 p=0.47) or between the wt yEP24 and wt pKF56 (p=0.13).

Figure 3. A. Lifespans of the wt (n=168) vs the *tsa1Δ* mutant (n=293), wt vs *tsa1C48S* (n=70), wt vs *tsa1C171S* (n=120), *tsa1ΔYF* (n=255) vs *tsa1ΔYFC171S* (n=70) are all different at p<0.00001. The lifespan of the *tsa1ΔYF* mutant is different from the wt at p<0.00854 whereas no significant difference was seen between the *tsa1Δ* vs *tsa1C48S* (p=0.11), *tsa1C48S* vs *tsa1C171S* (p=0.31), *tsa1ΔYFC171S* vs *tsa1C171S* (p=0.23). **C.** H_2O_2 resistance is significantly different between wt and *ras2Δ* strains (p=0.013), wt and *tsa1Δ* (p=0.0049) and *tsa1Δ* and *ras2Δ tsa1Δ* (p=0.010). **D.** H_2O_2 resistance is significantly different between wt control and o/e *TSA1* strains (p=0.0085), between wt o/e *TSA1* and *pde2Δ* o/e *TSA1* strains (p=0.0082) but not between *pde2Δ* control and o/e *TSA1* strains (p=0.56). **E.** H_2O_2 resistance is significantly different between wt vector and mc-*IRA2* strains (p=0.016), wt vector and *tsa1Δ* vector strains (p=0.049), *tsa1Δ* vector and mc-*IRA2* strains (p=0.00056), *tsa1Δ* mc-*IRA2* and *pde2Δtsa1Δ* mc-*IRA2* strains (p=0.0025) but neither the *pde2Δ* vector and mc-*IRA2* strains (p=0.40) nor *trx1Δ trx2Δ* vector and *trx1Δtrx2Δ* mc-*IRA2* strains (p=0.24). **F.** The scavenging rates of the wt and the *tsa1Δ* mutant following the addition of 0.4 mM are not significant in a two-tailed t-test assuming equal variance (p=0.684). **G.** Fluorescence ratios 500/420 nm of the HyPer3 expressing strains are significantly different between the wt young (n=231) vs old (n=319) (p=2.42 x 10^{-13}) and wt young vs wt young +H_2O_2 (n=202) (p=5.27 x 10^{-76}) but not when comparing wt old vs *tsa1Δ* old (n=236)(p=0.101). **H.** Fluorescence ratios 500/420 nm of the HyPer3 expressing strains are neither significantly different between the wt young (n=404) vs the o/e *TSA1* young (n=579, p=0.069) nor the wt old (n=190) vs o/e *TSA1* old (n=204, p=0.755). **I. ????**

Figure 4. C. The abundances of all the three T241-phosphorylated peptides decreased significantly upon adding either 0.4 mM or 0.8 mM H2O2 (for the C243-SH peptide p=0.05 and 0.037 respectively, for the C243-SSG peptide p=0.015 and 0.025 respectively whereas for the C243-SO_3H peptide p=0.011 and 0.0049, respectively. The quantity of the C243-SH T241 non-modified peptide did not change significantly upon the addition of 0.4 and 0.8 mM H_2O_2 (p=0.20 and 0.54, respectively) whereas the C243-SSG T241 non-modified peptide increased significantly following 0.4 mM (p=0.038) but not at 0.8 mM (p=0.17). **F.** Tpk1-S-SG levels are significantly different between wt with and without H_2O_2 (p=0.012), but not between wt and *tsa1Δ* without H_2O_2 (p=0.453) or in the *tsa1Δ* with and without H_2O_2 (p=0.264).

Figure 5. A. H_2O_2 resistance is significantly different between wt pRS313 vector control and *tpk2Δtpk3Δ* pRS313 vector control strains (p=0.030), *tpk1Δtpk2Δtpk3Δ pTPK1* and *ptpk1C243A*strains (p=0.030), *tpk1Δtpk2Δtpk3Δ pTPK1* and *ptpk1T241A* strains (p=0.0020) but not *tpk2Δtpk3Δ* pRS313 and *tpk1Δtpk2Δtpk3Δ pTPK1* strains (p=1.00). **B.** H_2O_2 resistance is significantly different between control *pTPK1* and *ptpk1C243A* strains (p=0.043), control *pTPK1* and *pTSA1 pTPK1* strains (p=0.0072), *pTSA1 pTPK1* and *ptpk1C243A* strains (p=0.0014) but not between control *ptpk1C243A* and *pTSA1*

ptpk1C243A strains (p=0.064). **C.** H_2O_2 resistance is significantly different between *TSA1 pTPK1* and *ptpk1T241A* strains (p=0.022), *TSA1 pTPK1* and *tsa1Δ pTPK1* strains (p=0.031), *tsa1Δ pTPK1* and *ptpk1T241A* strains (p=0.013) but not between *TSA1* and *tsa1Δ ptpk1T241A* strains (p=0.090).

Supplementary information

Figure 2 – figure supplement 1. Tsa1 and the cytosolic thioredoxins Trx1 and Trx2 impact on PKA related growth signaling but lack of Tsa1 cannot overcome the requirement for a PKA catalytic subunit for spore viability.

Figure 3 – figure supplement 1. Reduced Ras activity can overcome H_2O_2 sensitivity of cells lacking Tsa1 but not that of cell lacking the cytosolic thioredoxins Trx1 and Trx2.

Figure 4 – figure supplement 1. Tsa1 interacts with the PKA catalytic subunits Tpk1, controls Tpk1 cysteine sulfenylation independent on disulphide formation and a significant proportion of Tpk1 cysteines are glutathionylated under basal conditions.

Figure 5 – figure supplement 1. Substitution of Cys195, Thr241 and Cys243 by alanine in the yeast PKA catalytic subunit Tpk1 neither affects viability nor growth, whereas in silico simulation suggest that glutathionylation, but not sulfenylation, of Tpk1Cys243 significantly impacts on Tpk1 structure.

Supplementary file 1. Key resources table. Antibodies, chemicals, reagents, commercial assays, deposited data, yeast strains, oligonuycleotides, recombinant DNA and software and algorithms used.

Supplementary file 2. Tpk1 mass spectrometric data.

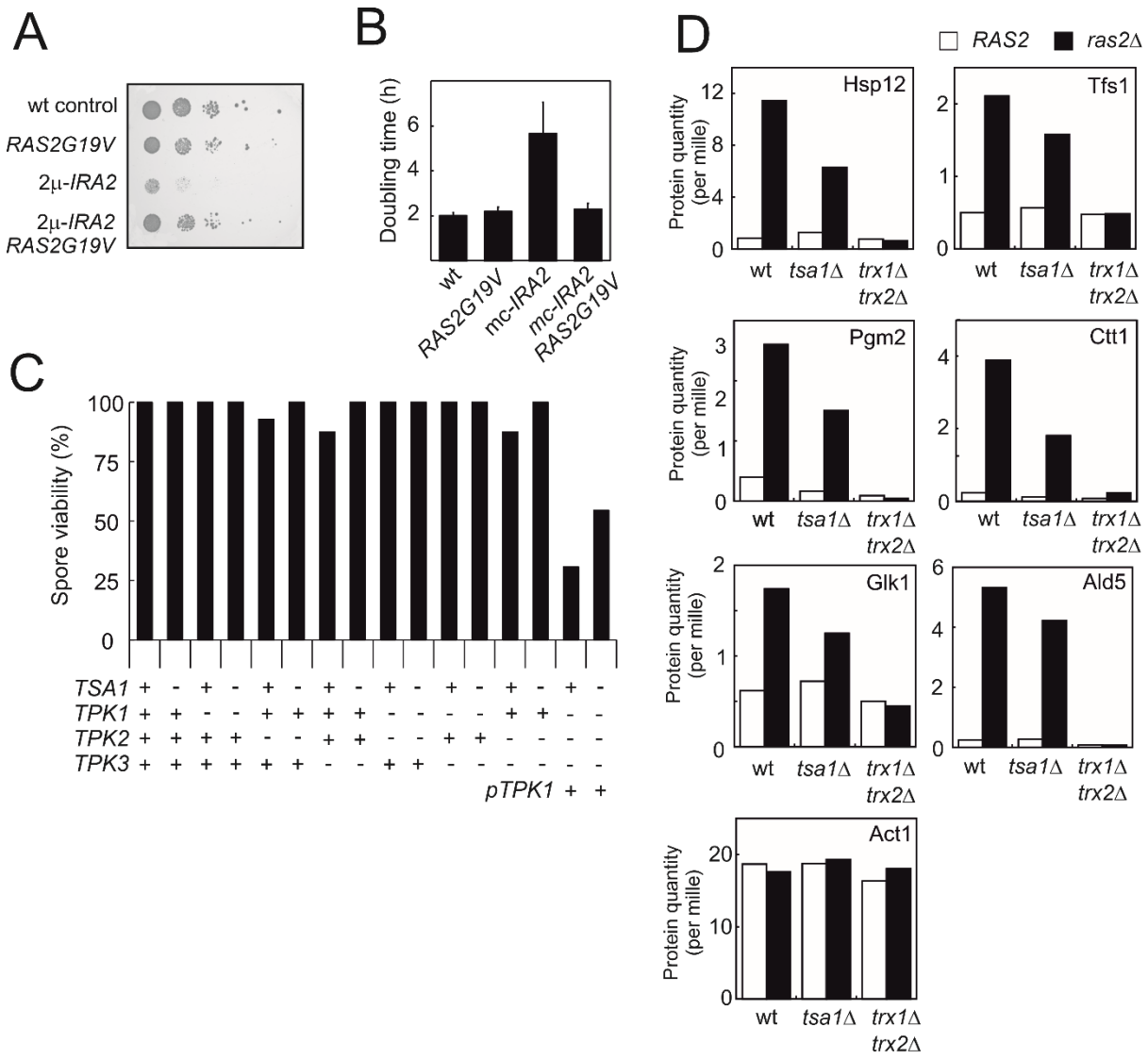

Figure 2 – figure supplement 1. Tsa1 and the cytosolic thioredoxins Trx1 and Trx2 impact on PKA related growth signaling but lack of Tsa1 cannot overcome the requirement for a PKA catalytic subunit for spore viability. **A-B.** Growth of cells expressing the oncogenic *RAS2G19V* allele, overexpressing *IRA2* (mc-*IRA2*) or both. **C.** Spore viability in mutants segregating in a *tsa1Δ* x *tpk1Δtpk2Δtpk3Δ* mutant cross. The *tpk1Δtpk2Δtpk3Δ* mutant was kept alive by a Tpk1-expressing plasmid (pRS313-*TPK1*). Spore viability was estimated in 43 tetrads where genotypes could be assigned to all spores (172 spores in total and in 8-15 spores per genotype). **D.** Expression of PKA repressed Msn2/4 targets (Hasan et al., 2002; Molin et al., 2011) in wild-type, *tsa1Δ* or *trx1Δtrx2Δ* cells deficient in *RAS2* (*ras2Δ*) or not (*RAS2*).

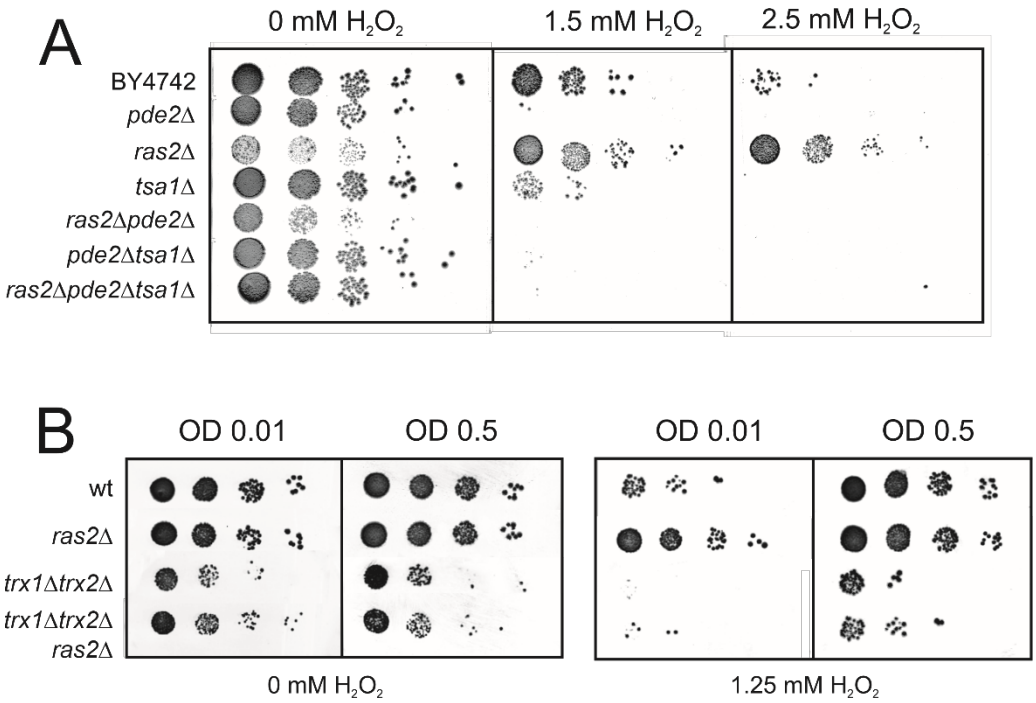

Figure 3 – figure supplement 1. Ras2-deficiency can overcome H_2O_2 sensitivity of cells lacking Tsa1, but not that of cell lacking the cytosolic thioredoxins Trx1 and Trx2, by reducing PKA signaling. **A.** H_2O_2 resistance in the indicated mutant strains strains grown to mid exponential phase (OD 0.3) and spotted onto plates with or without the indicated amounts of H_2O_2. **B.** H_2O_2 resistance in the indicated mutant strains strains grown to early (OD0.01) and mid exponential phase (OD0.5) and spotted onto plates with or without the indicated amounts of H_2O_2.

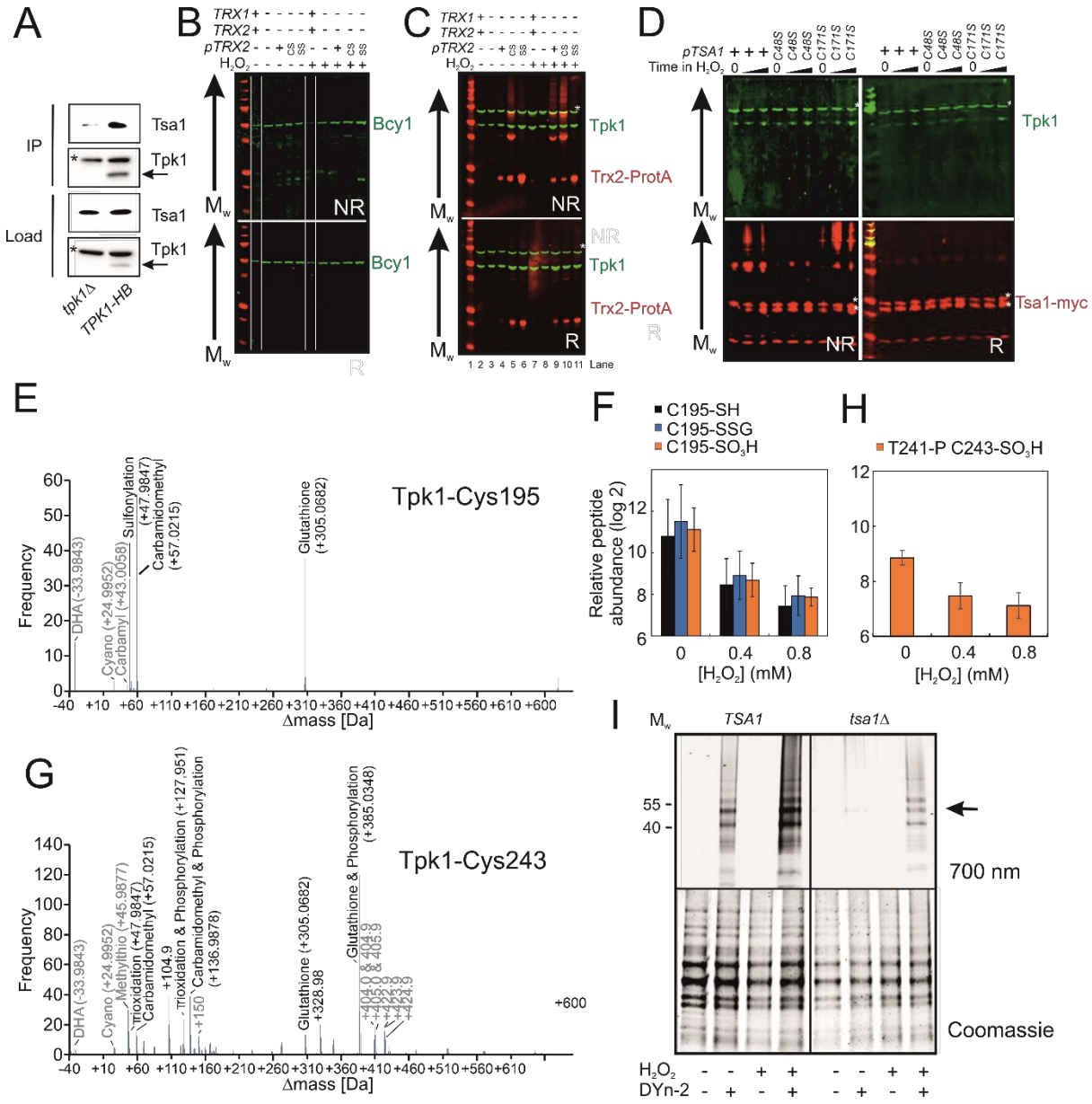

Figure 4 – figure supplement 1. Tsa1 interacts with the PKA catalytic subunits Tpk1, controls Tpk1 cysteine sulfenylation independent on disulphide formation and a significant proportion of Tpk1 cysteines are glutathionylated under basal conditions. **A.** Tsa1 interacts with Tpk1 in a Ni^{2+}-sepharose coimmunoprecipitation assay (Tpk1-HB *tpk2Δtpk3Δ* strain or *tpk1Δtpk3Δ* strain used as a negative control). An arrow indicates the Tpk1 specific band, whereas * indicates an unspecific band. **B-C)** Bcy1 (**B**) or Tpk1 (**C**) redox immunoblots of protein extracts isolated from the indicated thioredoxin mutant strains in the absence of stress (H_2O_2 -) or following the addition of 0.4 mM H_2O_2 for 20 min (H_2O_2 +). NR = non-reducing R = reducing CS = *trx2C34S* SS = *trx2C31SC34S*. **D)** Tpk1 redox immunoblots of protein extracts isolated from the indicated myc-*tsa1* mutant strains in the absence of stress (Time in H_2O_2 = 0) or 10 or 120 min following the addition of 0.4 mM H_2O_2. **E, G)** Mass-shifts in peptides covering the indicated Tpk1 cysteines detected using unbiased open search approaches. Tpk1-Cys195 denotes the F189-K204 peptide whereas Tpk1-Cys243 the Y239-K261 peptide. **F)** PRM-based quantification of the indicated C195 containing Tpk1 peptides (n=3). Error bars indicate SD. **H)** PRM-based quantification of the Thr241 phosphorylated and Cys243 sulfinic acid containing Y239-K261 peptide in Tpk1 (n=3). Error bars indicate SD. **I)** DYn-2 sulfenylation assay depicting oxidation of Tpk1 following the addition of 0.5 mM of H_2O_2 for 5 min or not in the presence and

absence of *TSA1*. Tpk1-HB was immunoprecipitated from *tpk2Δtpk3Δ* (*TSA1*) and *tpk2Δtpk3Δ tpk2Δtsa1Δ* (tsa1Δ) cells and analyzed in gel for cyanine5 fluorescence. Arrows indicate Tpk1. Coomassie staining was used to assess total protein used in the assay.

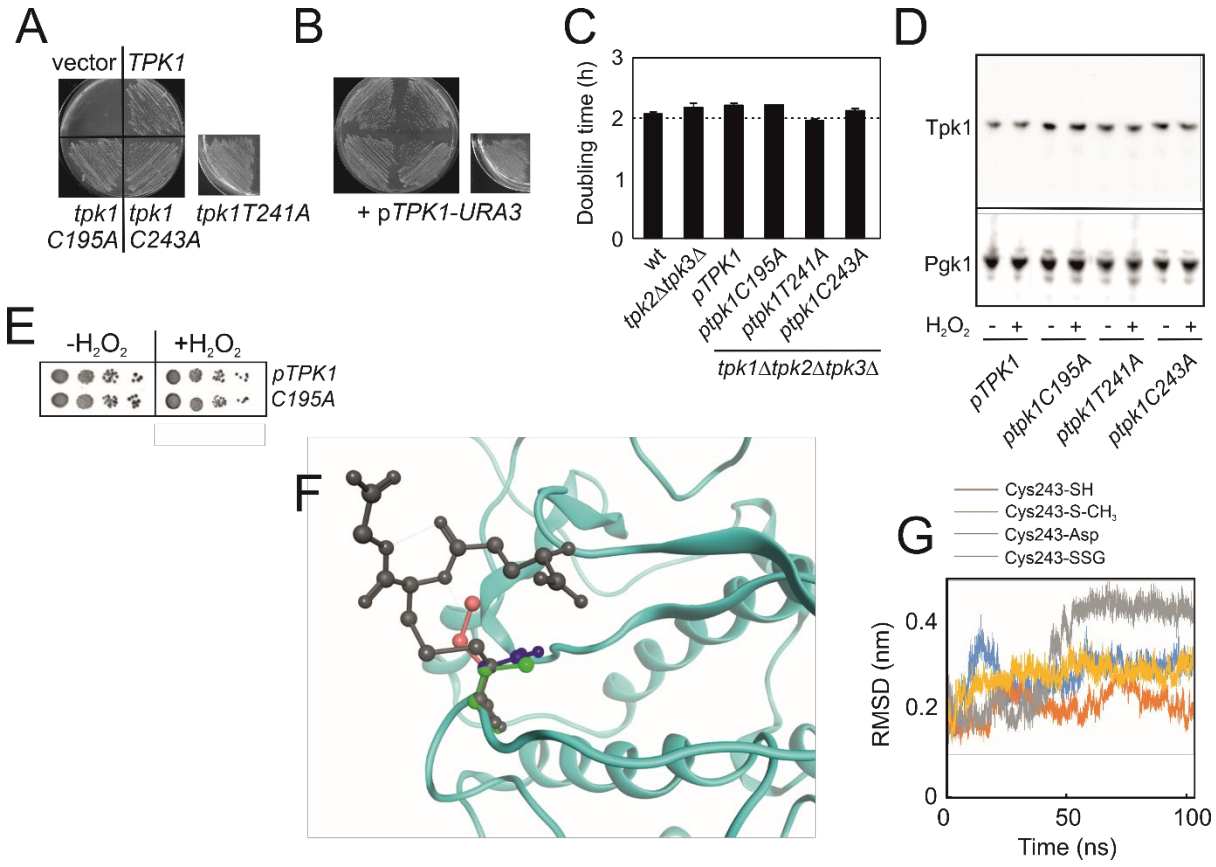

Figure 5 – figure supplement 1. Substitution of Cys195, Thr241 and Cys243 by alanine in the yeast PKA catalytic subunit Tpk1 neither affects viability nor growth, whereas *in silico* simulation suggest that glutathionylation, but not sulfenylation, of Tpk1Cys243 significantly impacts on Tpk1 structure. **A)** Growth of *tpk1Δtpk2Δtpk3Δ* cells transformed with the vector (vector) or the indicated pRS313-*TPK1* plasmids and pRS316-*TPK1* (p*TPK1-URA3*) on solid synthetic defined (-HIS, 5-FOA) medium to counterselect p*TPK1-URA3*. **B)** Growth of the strains in **A)** on solid synthetic defined selective (-HIS, URA) medium. Cells in **A)** and **B)** were left to grow for 3 days before photographed. **C)** Doubling time of the indicated *tpk*-mutant strains in synthetic defined -HIS medium. **D)** Tpk1 levels are not significantly altered in Tpk1 substitution mutants neither with nor without H_2O_2 (0.4 mM. 10 min). Pgk1 levels were used to indicate protein loading. **E)** H_2O_2 resistance of *TPK1 tpk2Δ tpk3Δ* and *tpk1C195A tpk2Δ tpk3Δ*-mutants as indicated. **F)** Alignment of cysteine (green), aspartate (blue), methylthiolated (pink) or glutathionylated cysteine (grey) in position 243 in the Tpk1 homology model. **G)** Root-mean-square deviation of the C-alpha distances in C243-SH (orange), Cys243Asp (blue), Cys243 methylthiolated (yellow) and C243 glutathionylated enzyme (Cys243-SSG, grey) upon molecular dynamic simulation.

Supplementary File 1. Key resources table

REAGENT or RESOURCE	SOURCE	IDENTIFIER
Antibodies		
Mouse monoclonal anti-Tpk1	Santa Cruz Biotechnology	Sc-374592, RRID: AB_10990730
Goat polyclonal anti-Bcy1	Santa Cruz Biotechnology	Sc-6734, RRID: AB_671758
Rabbit IgG (anti-ProtA)	Sigma Aldrich	I5006, RRID: AB_1163659
Goat polyclonal anti-Ras2	Santa Cruz Biotechnology	Sc-6759, RRID: AB_672465
Mouse monoclonal anti-Glutathione [D8]	Abcam	ab19534, RRID: AB_880243
Mouse monoclonal anti-Pgk1 [22C5D8]	Thermo Fisher	459250, RRID: AB_2532235
Mouse monoclonal anti-2 Cys Prx [6E5] (anti-Tsa1)	Abcam	ab16765, RRID: AB_443456
Bacterial and Virus Strains		
E. coli BL21 strain expressing pGEX2T-1-GST-RBD	This study, (Peeters et al., 2017)	
Chemicals, Peptides, and Recombinant Proteins		
G418	Acros Organics	Cat #: 329400050
ClonNAT	Werner Bioagents	Cat #: 5.005.000
Hygromycin B	Formedium	Cat #: HYG5000
Phleomycin	Sigma Aldrich	P9564
5-fluoroorotic acid	Sigma Aldrich	F5013
EZ-Link Sulfo-NHS-LC Biotin	Thermo Fisher	Cat #: 21335
Trichloroacetic acid	Sigma Aldrich	Cat #: T6399
KSCN	Sigma Aldrich	Cat #: P2713
$(NH_4)_2Fe(SO_4)_2 \cdot 6\ H2O$	Sigma Aldrich	Cat #: 215406
TRIzol Reagent	Thermo Fisher	Cat #: 15596026
DNase, RNase-free set	Qiagen	Cat #: 79254
cOmplete Mini EDTA-free protease inhibitor	Roche Applied Science	Cat #: 11873580001

Glutathione-S-Transferase-Raf1-Binding-Domain (GST-RBD)	This study, (Peeters et al., 2017)	
Glutathione Sepharose beads		
12% Bis-Tris NUPAGE gels	Thermo Fisher	Cat #: NP0349BOX
MOPS running buffer	Thermo Fisher	Cat #: NP0001
Immobilon-FL PVDF membrane	Millipore	Cat #: IPFL00010
Ni^{2+}-Sepharose beads	GE Healthcare	Cat #: 17-5318-06
Anti-c-myc, agarose conjugated	Sigma-Aldrich	Cat #: A7470
Trypsin Gold, mass spectrometry grade	Promega	Cat #: V5280
N-ethylmaleimide	Sigma-Aldrich	Cat #: E3876
DYn-2	Cayman Chemical	Cat #: 11220
10% Criterion TGX Precast Midi Protein Gel	Bio-Rad	Cat #: 5671034
Peptide Retention Time Calibration Mixture	Pierce, Thermo Fisher	Cat #: 88320
Critical Commercial Assays		
PureLink RNA Mini kit	Thermo-Fisher	Cat #: 12183025
QuantiTect Reverse Transcription Kit	Qiagen	Cat #: 205313
iQ SYBR Green Supermix	BioRad	Cat #: 170-8882
LANCE cAMP 384 kit	Perkin Elmer	Cat #: AD0262
Deposited Data		
Tpk1 MS-data	PRIDE	PXD012617
Yeast strains used		
YMM130, wt control	(Hanzen et al., 2016)	MAT **alpha** *his3Δ1::pRS403, leu2Δ0 lys2Δ0 ura3Δ0*
o/e *TSA1*	(Hanzen et al., 2016)	MAT **alpha** *his3Δ1::pRS403-Myc-TSA1, leu2Δ0 lys2Δ0 ura3Δ0*

YMM175, *pde2Δ control*	This study	MAT **alpha** *his3Δ1::pRS403, leu2Δ0 lys2Δ0 ura3Δ0 pde2Δ::kanMX4*
YMM176, *pde2Δ* o/e *TSA1*	This study	MAT **alpha** *his3Δ1::pRS403-Myc-TSA1, leu2Δ0 lys2Δ0 ura3Δ0 pde2Δ::kanMX4*
BY4742, wt	(Brachmann et al., 1998)	MAT **alpha** *his3Δ1 leu2Δ0 lys2Δ0 ura3Δ0*
YMM114, *tsa1Δ*	(Molin et al., 2011)	BY4742 *tsa1Δ::natMX4*
YMM113, *ras2Δ*	(Molin et al., 2011)	BY4742 *ras2Δ::kanMX4*
YMM170, *ras2Δtsa1Δ*	This study	BY4742 *ras2Δ::kanMX4 tsa1Δ::natMX4*
BY4742, *pde2Δ*	Research Genetics, (Giaever et al., 2002)	BY4742 *pde2Δ::kanMX4*
YMM171, *ras2Δpde2Δ*	This study	BY4742 *ras2Δ::kanMX4 pde2Δ::hphMX4*
YMM172, *pde2Δtsa1Δ*	This study	BY4742 *pde2Δ::kanMX4 tsa1Δ::natMX4*
YMM173, *ras2Δpde2Δtsa1Δ*	This study	BY4742 *ras2Δ::kanMX4 pde2Δ::hphMX4 tsa1Δ::natMX4*
YMM145, *tsa1C48S*	(Bodvard et al., 2017)	BY4742 *tsa1C48S*
YMM146, *tsa1C171S*	(Bodvard et al., 2017)	BY4742 *tsa1C171S*
YMM147, *tsa1ΔYF*	(Bodvard et al., 2017)	BY4742 *tsa1(1-184)*
YMM148, *tsa1C171SΔYF*	(Bodvard et al., 2017)	BY4742 *tsa1(1-184)C171S*

YMM143, *trx1Δtrx2Δ*	(Bodvard et al., 2017)	BY4742 *trx1Δ::hphMX4* *trx2Δ::natMX4*
YMM174, *msn2Δmsn4Δ*	This study	BY4742 *msn2Δ::hphMX4* *msn4Δ::natMX4*
YMM177	This study	**MAT a**, *his3Δ1* *leu2Δ0 lys2Δ0 ura3Δ0* *ras1Δ::hphMX4*
YMM178	This study	BY-2n *met15Δ0/MET15* *lys2Δ0/LYS2* *tpk1Δ::kanMX4/TPK1* *tpk2Δ::natMX4/TPK2* *tpk3Δ::hphMX4/TPK3*
YMM179, *tpk1Δtpk3Δ*	This study	BY4742 *tpk1Δ::kanMX4* *tpk3Δ::hphMX4*
YMM180, *tpk2Δtpk3Δ*	This study	BY4742 *tpk2Δ::natMX4* *tpk3Δ::hphMX4*
YMM181, *tpk1Δtpk2Δtpk3Δ pTPK1-URA*	This study	BY4742 *tpk1Δ::kanMX4* *tpk2Δ::natMX4* *tpk3Δ::hphMX4* *pRS316-TPK1*
YMM182, *tpk1Δtpk2Δtpk3Δ pTPK1-URA vector control*	This study	BY4742 *tpk1Δ::kanMX4* *tpk2Δ::natMX4* *tpk3Δ::hphMX4* *pRS313 pTPK1-URA3*
YMM183, *tpk1Δtpk2Δtpk3Δ pTPK1-URA pTPK1*	This study	BY4742 *tpk1Δ::kanMX4* *tpk2Δ::natMX4* *tpk3Δ::hphMX4* *pRS313-TPK1 pTPK1-URA3*
YMM184, *tpk1Δtpk2Δtpk3Δ pTPK1-URA3 ptpk1C243A*	This study	BY4742 *tpk1Δ::kanMX4* *tpk2Δ::natMX4* *tpk3Δ::hphMX4* *pRS313-tpk1C243A* *pTPK1-URA3*

YMM185, *tpk1Δtpk2Δtpk3Δ pTPK1-URA3 ptpk1C243D*	This study	BY4742 *tpk1Δ::kanMX4* *tpk2Δ:natMX4* *tpk3Δ::hphMX4* *pRS313-tpk1C243D* *pTPK1-URA3*
YMM186, *tpk1Δtpk2Δtpk3Δ pTPK1-URA3 ptpk1T241A*	This study	BY4742 *tpk1Δ::kanMX4* *tpk2Δ::natMX4* *tpk3Δ::hphMX4* *pRS313-tpk1T241A* *pTPK1-URA3*
YMM187, *tpk1Δtpk2Δtpk3Δ pTPK1*	This study	BY4742 *tpk1Δ::kanMX4* *tpk2Δ::natMX4* *tpk3Δ::hphMX4* *pRS313-TPK1*
YMM188, *tpk1Δtpk2Δtpk3Δ ptpk1C243A*	This study	BY4742 *tpk1Δ::kanMX4* *tpk2Δ::natMX4* *tpk3Δ::hphMX4* *pRS313-tpk1C243A*
YMM189, *tpk1Δtpk2Δtpk3Δ ptpk1C243D*	This study	BY4742 *tpk1Δ::kanMX4* *tpk2Δ::natMX4* *tpk3Δ::hphMX4* *pRS313-tpk1C243D*
YMM190, *tpk1Δtpk2Δtpk3Δ ptpk1T241A*	This study	BY4742 *tpk1Δ::kanMX4* *tpk2Δ::natMX4* *tpk3Δ::hphMX4* *pRS313-tpk1T241A*
YMM191, *ras2Δtrx1Δtrx2Δ*	This study	BY4742 *ras2Δ::kanMX4* *trx1Δ::hphMX4* *trx2Δ::natMX4*
YMM192	This study	BY4741 *tsa1Δ::bleMX4*
YMM193, *tpk2Δtpk3Δtsa1Δ*	This study	BY4741 *tpk2Δ::natMX4* *tpk3Δ::hphMX4* *tsa1Δ::bleMX4*

WR1832, *TPK1-HBH tpk2Δtpk3Δ*	This study	BY4742 *TPK1-HBH::TRP1 tpk2Δ::natMX4 tpk3Δ::hphMX4 trp1Δ::kanMX4*
yCP101, *tpk1Δtpk2Δtpk3Δ pTPK1-URA vector control*	This study	MAT **a** *his3Δ1::pRS403, leu2Δ0 lys2Δ0 ura3Δ0 tpk1Δ::kanMX4 tpk2Δ::natMX4 tpk3Δ::hphMX4 pRS316-TPK1*
yCP102, *tpk1Δtpk2Δtpk3Δ ptpk1C243A-URA vector control*	This study	MAT **alpha** *his3Δ1::pRS403, leu2Δ0 lys2Δ0 ura3Δ0 tpk1Δ::kanMX4 tpk2Δ::natMX4 tpk3Δ::hphMX4 pRS316-tpk1C243A*
yCP103, *tpk1Δtpk2Δtpk3Δ pTPK1-URA* o/e *TSA1*	This study	MAT **alpha** *his3Δ1::pRS403-myc-TSA1, leu2Δ0 lys2Δ0 ura3Δ0 tpk1Δ::kanMX4 tpk2Δ::natMX4 tpk3Δ::hphMX4 pRS316-TPK1*
yCP104, *tpk1Δtpk2Δtpk3Δ ptpk1C243A-URA* o/e *TSA1*	This study	MAT **alpha** *his3Δ1::pRS403-myc-TSA1, leu2Δ0 lys2Δ0 ura3Δ0 tpk1Δ::kanMX4 tpk2Δ::natMX4 tpk3Δ::hphMX4* pRS316-*tpk1C243A*
yCP105, *tpk1Δtpk2Δtpk3Δtsa1Δ pTPK1*	This study	BY4742 *tpk1Δ::kanMX4 tpk2Δ::natMX4 tpk3Δ::hphMX4 tsa1Δ::bleMX4 pRS313-TPK1*

yCP106, *tpk1Δtpk2Δtpk3Δtsa1Δ ptpk1T241A*	This study	BY4742 *tpk1Δ::kanMX4 tpk2Δ::natMX4 tpk3Δ::hphMX4 tsa1Δ::bleMX4 pRS313-tpk1T241A*
yCP107, *TPK1-HBH tpk2Δtpk3Δtsa1Δ*	This study	BY4742 *TPK1-HBH::TRP1 tpk2Δ::natMX4 tpk3Δ::hphMX4 trp1Δ::kanMX4 tsa1Δ::bleMX4*
Oligonucleotides		
ACT1F	(Caballero et al., 2011)	For Q-PCR of *ACT1* CTGCCGGTATTG ACCAAACT
ACT1R	(Caballero et al., 2011)	For Q-PCR of *ACT1* CGGTGAATTTCC TTTTGCATT
CTT1F	This study	For Q-PCR of *CTT1* GCTTCTCAATAC TCAAGACCAG
CTT1R	This study	For Q-PCR of *CTT1* GCGGCGTATGTA ATATCACTC
HSP12F	(Caballero et al., 2011)	For Q-PCR of *HSP12* AGGTCGCTGGTA AGGTTC
HSP12R	(Caballero et al., 2011)	For Q-PCR of *HSP12* ATCGTTCAACTT GGACTTGG
Recombinant DNA		
yEP24	(Botstein et al., 1979)	yeast 2μ, *URA3* vector
pKF56	(Tanaka et al., 1990)	*IRA2* in yEP24
pRS425	(Christianson, Sikorski, Dante, Shero, & Hieter, 1992)	yeast 2μ, *LEU2* vector

yEP13-*PDE2*	(Hlavata, Aguilaniu, Pichova, & Nystrom, 2003)	*PDE2* in yeast 2µ, *LEU2* plasmid
yEPlac195	(Gietz & Sugino, 1988)	yeast 2µ, *URA3* vector
pXP1	(Pan & Heitman, 1999)	*BCY1* in yEPlac195
pRS315	(Sikorski & Hieter, 1989)	yeast CEN/ARS, *LEU2* empty vector
B561 (pRS315-*RAS2G19V*)	(Bartels, Mitchell, Dong, & Deschenes, 1999)	*RAS2G19V* in pRS315
pHyPer3C199S (pRS416-*GPD-HyPer3C199S*)	This study, (Bilan et al., 2013)	HyPer3C199S
pRS416-*GPD-AKAR4*	(Molin et al., 2020)	AKAR4 in pRS416-GPD [CEN/ARS, pGPD promotor, *URA3*]
pRS316	(Sikorski & Hieter, 1989)	yeast CEN/ARS, *URA3* empty vector
pRS316- *myc-TSA1*	(Biteau, Labarre, & Toledano, 2003)	Myc-*TSA1* in pRS316
pRS316- *myc-tsa1C48S*	(Molin et al., 2011)	Myc-*tsa1C48S* in pRS316
pRS316- *myc-tsa1C171S*	(Molin et al., 2011)	Myc-*tsa1C171S* in pRS316
pRS315-ProtA	This study	ProteinA in pRS315
pRS315-*TRX2-ProteinA*	(Bodvard et al., 2017)	*TRX2-ProtA* in pRS315
pRS315-*trx2C34S-ProteinA*	This study	*trx2C34S-ProtA* in pRS315
pRS315-*trx2C31SC34S-ProteinA*	This study	*trx2C31SC34S-ProtA* in pRS315
pRS313	(Sikorski & Hieter, 1989)	yeast CEN/ARS, *HIS3* empty vector
pRS313-*TPK1*	(Voordeckers et al., 2011)	*TPK1* in pRS313
pRS313-*tpk1C243A*	This study	*tpk1C243A* in pRS313
pRS313-*tpk1C243D*	This study	*tpk1C243D* in pRS313
pRS313-*tpk1T241A*	This study	*tpk1T241A* in pRS313
p*TPK1-URA3 (*pRS316-*TPK1)*	Karin Voordeckers	*TPK1* in pRS316

p*tpk1C243A-URA3*	This study	*tpk1C243A* in pRS316
Software and Algorithms		
MATLAB	Mathworks	version 2016b
CellX	(Mayer, Dimopoulos, Rudolf, & Stelling, 2013)	
Scrödinger Suite	Schrödinger LLC	
GROMACS	(Abraham et al., 2015)	
Amber tools	(Salomon-Ferrer, Case, & Walker, 2013)	

Supplementary file 1 references

Abraham, M. J., Murtola, T., Schultz, R., Pall, S., Smith, J. C., Hess, B., & Lindahl, E. (2015). GROMACS: High performance molecular simulations through multi-level parallelism from laptops to supercomputers. *SoftwareX, 54*(7), 1932-1940.

Bartels, D. J., Mitchell, D. A., Dong, X., & Deschenes, R. J. (1999). Erf2, a novel gene product that affects the localization and palmitoylation of Ras2 in Saccharomyces cerevisiae. *Mol Cell Biol, 19*(10), 6775-6787.

Bilan, D. S., Pase, L., Joosen, L., Gorokhovatsky, A. Y., Ermakova, Y. G., Gadella, T. W. J., . . . Belousov, V. V. (2013). HyPer-3: A Genetically Encoded H2O2 Probe with Improved Performance for Ratiometric and Fluorescence Lifetime Imaging. *ACS chemical biology, 8*(3), 535-542. doi:10.1021/cb300625g

Biteau, B., Labarre, J., & Toledano, M. B. (2003). ATP-dependent reduction of cysteine-sulphinic acid by *S. cerevisiae* sulphiredoxin. *Nature, 425*(6961), 980-984.

Bodvard, K., Peeters, K., Roger, F., Romanov, N., Igbaria, A., Toledano, M. B., . . . Molin, M. (2017). Light-sensing via hydrogen peroxide and a peroxiredoxin. *Nat Commun, 8*, 14791. doi:10.1038/ncomms14791

Botstein, D., Falco, S. C., Stewart, S. E., Brennan, M., Scherer, S., Stinchcomb, D. T., . . . Davis, R. W. (1979). Sterile host yeasts (SHY): a eukaryotic system of biological containment for recombinant DNA experiments. *Gene, 8*(1), 17-24.

Brachmann, C. B., Davies, A., Cost, G. J., Caputo, E., Li, J., Hieter, P., & Boeke, J. D. (1998). Designer deletion strains derived from *Saccharomyces cerevisiae* S288C: a useful set of strains and plasmids for PCR-mediated gene disruption and other applications. *Yeast, 14*(2), 115-132.

Caballero, A., Ugidos, A., Liu, B., Oling, D., Kvint, K., Hao, X., . . . Nystrom, T. (2011). Absence of mitochondrial translation control proteins extends life span by activating sirtuin-dependent silencing. *Molecular cell, 42*(3), 390-400. doi:10.1016/j.molcel.2011.03.021

Christianson, T. W., Sikorski, R. S., Dante, M., Shero, J. H., & Hieter, P. (1992). Multifunctional yeast high-copy-number shuttle vectors. *Gene, 110*(1), 119-122. doi:0378-1119(92)90454-W [pii]

Giaever, G., Chu, A. M., Ni, L., Connelly, C., Riles, L., Veronneau, S., . . . Johnston, M. (2002). Functional profiling of the *Saccharomyces cerevisiae* genome. *Nature, 418*(6896), 387-391.

Gietz, R. D., & Sugino, A. (1988). New yeast-*Escherichia coli* shuttle vectors constructed with in vitro mutagenized yeast genes lacking six-base pair restriction sites. *Gene, 74*(2), 527-534.

Hanzen, S., Vielfort, K., Yang, J., Roger, F., Andersson, V., Zamarbide-Fores, S., . . . Nystrom, T. (2016). Lifespan Control by Redox-Dependent Recruitment of Chaperones to Misfolded Proteins. *Cell, 166*(1), 140-151. doi:10.1016/j.cell.2016.05.006

Hlavata, L., Aguilaniu, H., Pichova, A., & Nystrom, T. (2003). The oncogenic RAS2(val19) mutation locks respiration, independently of PKA, in a mode prone to generate ROS. *Embo J, 22*(13), 3337-3345. doi:10.1093/emboj/cdg314

Mayer, C., Dimopoulos, S., Rudolf, F., & Stelling, J. (2013). Using CellX to Quantify Intracellular Events. *101*(1), 14.22.11-14.22.20. doi:doi:10.1002/0471142727.mb1422s101

Molin, M., Logg, K., Bodvard, K., Peeters, K., Forsmark, A., Roger, F., . . . Blomberg, A. (2020). cAMP-dependent protein kinase controls the multifacteted biology of visible light. *BMC Biology, under review*.

Molin, M., Yang, J., Hanzen, S., Toledano, M. B., Labarre, J., & Nystrom, T. (2011). Life span extension and H_2O_2-resistance elicited by caloric restriction require the peroxiredoxin Tsa1 in *Saccharomyces cerevisiae*. *Mol Cell, 43*(5), 823-833. doi:10.1016/j.molcel.2011.07.027

Pan, X., & Heitman, J. (1999). Cyclic AMP-dependent protein kinase regulates pseudohyphal differentiation in Saccharomyces cerevisiae. *Mol Cell Biol, 19*(7), 4874-4887.

Peeters, K., Van Leemputte, F., Fischer, B., Bonini, B. M., Quezada, H., Tsytlonok, M., . . . Thevelein, J. M. (2017). Fructose-1,6-bisphosphate couples glycolytic flux to activation of Ras. *Nat Commun, 8*(1), 922. doi:10.1038/s41467-017-01019-z

Salomon-Ferrer, R., Case, D. A., & Walker, R. C. (2013). An overview of the Amber biomolecular simulation package. *Wiley Interdisciplinary Reviews-Computational Molecular Science, 3*(2), 198-210. doi:10.1002/wcms.1121

Sikorski, R. S., & Hieter, P. (1989). A system of shuttle vectors and yeast host strains designed for efficient manipulation of DNA in *Saccharomyces cerevisiae*. *Genetics, 122*(1), 19-27.

Tanaka, K., Nakafuku, M., Tamanoi, F., Kaziro, Y., Matsumoto, K., & Toh-e, A. (1990). IRA2, a second gene of Saccharomyces cerevisiae that encodes a protein with a domain homologous to mammalian ras GTPase-activating protein. *Mol Cell Biol, 10*(8), 4303-4313.

Voordeckers, K., Kimpe, M., Haesendonckx, S., Louwet, W., Versele, M., & Thevelein, J. M. (2011). Yeast 3-phosphoinositide-dependent protein kinase-1 (PDK1) orthologs Pkh1-3 differentially regulate phosphorylation of protein kinase A (PKA) and the protein kinase B (PKB)/S6K ortholog Sch9. *J Biol Chem, 286*(25), 22017-22027. doi:10.1074/jbc.M110.200071